Geysers Caused by the Sudden Release of Pressurized Air Pockets

by

Kathleen Zeaser Muller

A thesis submitted to the Graduate Faculty of
Auburn University
in partial fulfillment of the
requirements for the Degree of
Master of Science

Auburn, Alabama
May 6, 2017

Keywords: geyser, stormwater, physical modeling, stormwater systems, air-water flows, geysering

Approved by

Jose Goes Vasconcelos, Associate Professor of Civil Engineering
Prabhakar Clement, Groome Endowed Professor of Environmental Engineering
Xing Fang, Arthur H. Feagin Chair Professor of Civil Engineering

Abstract

Uncontrolled air pockets released from water-filled shafts can lead to geysering in stormwater systems. Such occurrences are deleterious from public health and environmental standpoint and can cause property and structural damage. Causes, frequency, magnitude, and location of geysering events are still poorly understood, and pose practical difficulties to designers as to how to create drop shafts that are less likely to present this issue. This work presents results from experimental and numerical investigations on air-related geysers that aimed to gain insight on the mechanisms of air release and the displacement of water in vertical shafts. A $302\,mm$ schedule 40 clear PVC apparatus was constructed with the essential features of a stormwater tunnel, and was fitted with vertical shafts with diameters ranging from $0.10\,m$ to $0.20\,m$. During these experiments, predetermined air pocket volumes were released in the horizontal pipe, and eventually reached shafts causing water displacement and often geysers. Kinematics of the air pocket release were measured along with pressures at selected points in the apparatus. These results were used in the calibration of a CFD model based on OpenFOAM, which compared well with the experimental measurements. The model was subsequently used in a larger geometry that allowed the evaluation of air pocket release kinematics for a wider range of conditions. Findings of this work provide further details on the nature and strength of geysering events, and suggestions for future studies in this topic are also provided.

Acknowledgments

I would like to thank my adviser, Dr. Vasconcelos for his continued support and everything he has done to help me earn my degrees. I would also like to thank LimnoTech for financially supporting this project and the Alabama Supercomputer Authority for supporting the CFD model execution.

LIST OF ABBREVIATIONS

D	=	Shaft Diameter (m)
D^*	=	Normalized Shaft Diameter
D_t	=	Tunnel Diameter (m)
g	=	Gravity acceleration(m/s^2)
L	=	Length of vertical shaft (m)
t	=	Time(s)
V_{air}	=	Air Pocket Volume (L)
V^*_{air}	=	Normalized air pocket volume
V_{Int}	=	Velocity of the air-water interface (m/s)
V^*_{Int}	=	Normalized velocity of the air-water interface
V_{FS}	=	Velocity of the free surface (m/s)
V^*_{FS}	=	Normalized velocity of the free surface
Y_{Int}	=	Vertical coordinate of the air-water interface in the vertical shaft (m)
Y^*_{Int}	=	Normalized vertical coordinate of the air-water interface in the vertical shaft
Y_{FS}	=	Vertical coordinate of the free surface in the vertical shaft (m)
Y^*_{FS}	=	Normalized vertical coordinate of the free surface in the vertical shaft

List of Figures

List of Tables

Table of Contents

Chapter 1

Introduction

As more people relocate from rural areas to more densely populated areas, urbanization and land development progresses, leading to changes in land use and hydrological characteristics of watersheds. The most common changes observed are increased runoff peak, runoff volume, and reduced time to peak flow [Goonetilleke et al., 2005]. Where there was once a pasture, there is now a parking lot or a roadway. Where there was once a baseball field, there is now a shopping mall. Where rainfall once infiltrated into the ground and became part of the groundwater, it now creates overland flow. As the land is developed and highly pervious surfaces like forests and grasslands are replaced with impervious surfaces such as concrete and pavement, water collection systems with higher capacities are now necessary to relocate this excess runoff. Even these systems may be overwhelmed by severe rain events, requiring relief by some type of stormwater storage approach.

Parallel to increased runoff volume issues, there are also other issues related to stormwater quality. Urban stormwater runoff introduces various types of pollutants to receiving water bodies [Goonetilleke et al., 2005]. The result is damage to aquatic habitats caused by altering the ecosystem, changing the natural state of water bodies, among other problems. This is particularly the case in combined stormwater/sanitary sewer systems, which are systems that convey stormwater, domestic sewage, and industrial waste in the same pipe, as shown in Figure 1.1. During most rain events, stormwater and wastewater in combined sewer systems is collected and routed to wastewater treatment plants where it is treated to reduce pollutants before it is discharged into a receiving water body. Intense rain events can exceed the capacity of the sewer collection system, triggering combined sewer overflow (CSO), defined as spills of untreated discharges into natural water bodies [Shammas and Wang, 2011].

Figure 1.1: Diagram of a combined sewer system from the Huntington Sanitary Board

As urbanization increases for areas with combined sewer systems, large runoff volumes can pressurize the flow in sewers and potentially lead to more frequent overflow episodes.

To counter environmental impacts created by human activities in watersheds, including CSO events, the United States Environmental Protection Agency (EPA) has put forth The Federal Water Pollution Control Act (Clean Water Act) in an effort to protect public health and the environment. This act prohibits the discharge of pollutants to waters of the United States from any point source other than those permitted by the National Pollution Discharge Elimination System (NPDES) [Augustenborg and Duke , 2001]. This means that any discharge of pollutants into United States water bodies must have a NPDES permit, including but not limited to: pipes, ditches, channels, tunnels, conduits, or containers [Cook and DeBell, 2002]. Since this act has gone into effect, billions of pounds of pollutants have

been stopped from entering the waterways. Yet forty percent of the nation's waterbodies are still unsafe for recreational uses [Cook and DeBell, 2002]. Although point source pollution sources have been partially eliminated or controlled, there is still pollution caused by non-point sources such as urban runoff. Some of the most prevalent urban runoff pollutants are sediments, nutrients, pathogens, heavy metals, organics, and salts which are associated with various land uses such as construction, agriculture, roadway use, etc. [Shammas and Wang, 2011].

1.1 Providing Relief to Stormwater Systems

As a result, there have been practices proposed to provide relief for stormwater collection systems and prevent untreated sewage discharge. For lightly urbanized areas, relief for overwhelmed drainage systems can be provided by grade-level reservoirs (e.g. detention basins) next to a development. For highly urbanized areas, where there is not available land to be used for this purpose, there are fewer effective strategies. One is to control the inflow into the system by storing the water in below-grade reservoirs. Such reservoirs are constructed with concrete or plastic just below the ground surface. During a major storm event, excess storm water is stored there until it can be discharged gradually as to not exceed the capacity of the drainage systems. These underground reservoirs are also useful for improving the water quality because they act as settling basins. When the velocity of the water significantly decreases, some of the suspended particles fall to the bottom of the tank. As a result, there are maintenance requirements, and the tanks need to be accessible in order to be cleaned.

One dramatic case of issues with stormwater systems was the city of Chicago, which was having major problems with CSO discharge. The pipes were aged and undersized for the amount of urbanization that has occurred in the city over the last few decades. When there was a rain event, it caused the combined system to overflow into the surrounding water

bodies in 600 locations for more than 100 days per year (EPA website). This problem was so severe that when storms were large, the direction of the rivers was reversed (EPA website).

The area became so polluted that sewage would back up into homes, aquatic life vanished, and the shoreline along Lake Michigan (the source of drinking water) was frequently off limits for recreational purposes. In 1972 the city developed the Tunnel and Reservoir Plan (TARP) in order to conform to the Federal and State water quality standards, to protect Lake Michigan, and to reduce flooding in the city. Their strategy is as follows: stormwater is collected in large-dimension below-grade stormwater tunnels. As there is capacity in the water reclamation plant, the stormwater is pumped from the tunnels to the plant, making room in the tunnels for the next rain event. This phase has been completed. The phase in progress is 3 large reservoirs that will together store 20.5 billion gallons (about 775,000 m^3) of CSO during stormwater events, saving over $130 million in annual flood damage and protect $1.5 million structures from flooding (EPA website). Figure 1.2 shows a map of the current project status of the TARP project in Chicago.

While designated to address CSO issues, the tunnels created other issues. One operational problem in multiple stormwater systems, including Chicago's TARP, is the occurrence of stormwater geysers, defined by Vasconcelos and Wright [2011] as the return of conveyed water from sewers and storage tunnel systems back to grade in an uncontrolled fashion. Often times, such occurrences are characterized by jets of air-water mix rising through manholes and other vertical structures. With air-water mixtures traveling rapidly and forcefully through vertical shafts, their occurrence can be very damaging and result in a number of deleterious impacts such as excessive surging, overflows, large pressures, manhole lid displacements, among others. In such conditions, these systems can contribute to negative impacts to the environment and public health as well as costs associated with related structural damage. While relevant, research towards better understanding this phenomenon and implementing mitigation techniques is very limited.

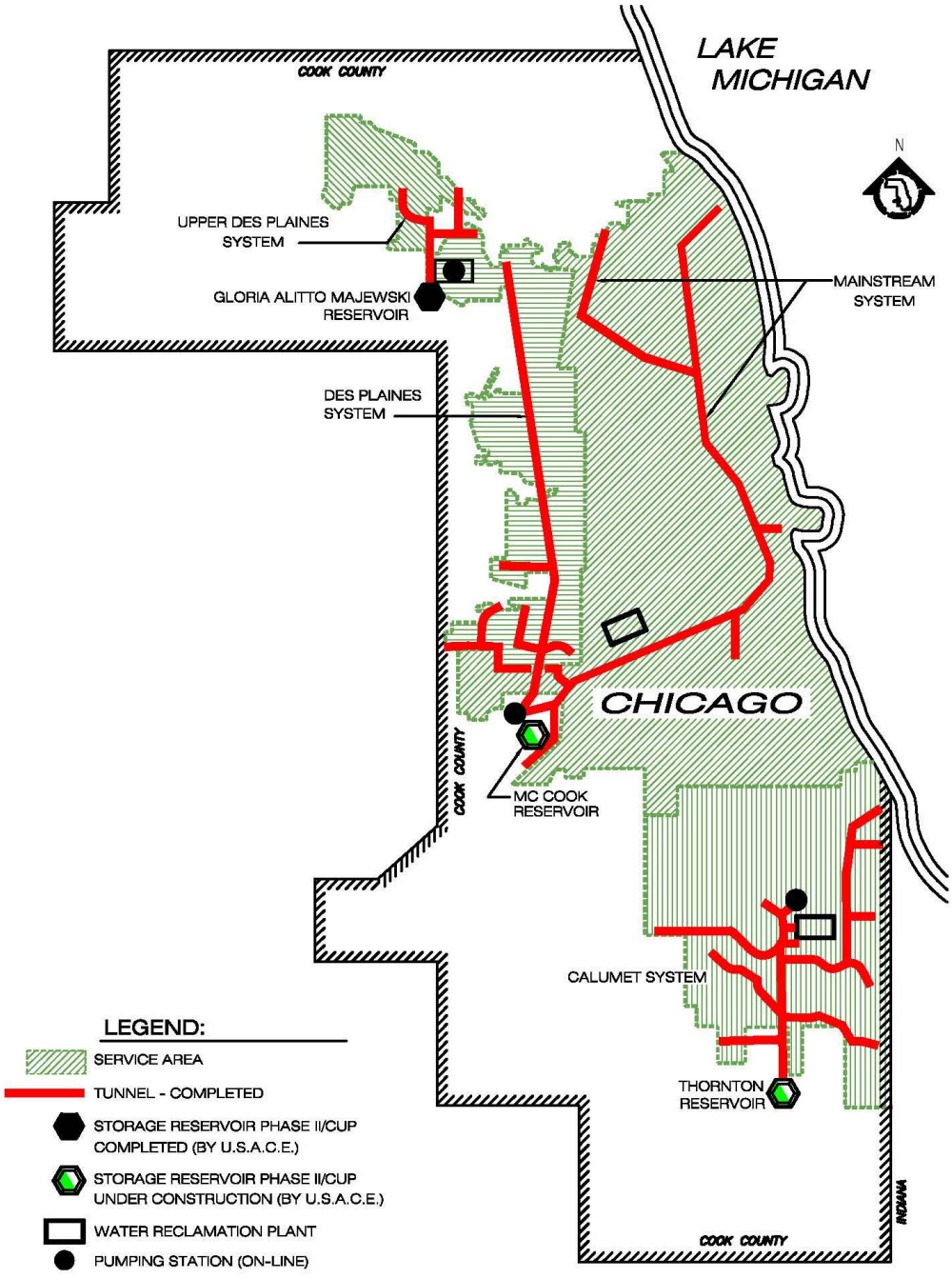

Figure 1.2: Map of current progress for Chicago's TARP from

Chapter 2

Literature Review

This chapter summarizes past research and knowledge related to air pocket formation, horizontal and vertical air pocket motion, and how this impacts stormwater systems. This is followed by an introduction to the relevance of these topics to geyser formation and occurrence as well as knowledge gaps within the subject area.

2.1 Operational Issues Linked to Rapid Filling of Stormwater Tunnels

Stormwater systems can present a variety of operational problems when subjected to rapid inflow conditions associated with intense rain events. Such operational problems include excessive surging, overflows, large pressures, manhole lid displacements, among others. In such conditions, such systems can create negative impacts to the environment and public health, as well costs associated with related structural damages. The presence of large, entrapped air pockets in stormwater systems have the potential of worsening some of these problems. For instance, if entrapped air accumulates at a high point within the tunnel system, there will be a partial blockage of flow, reducing the capacity of the system. The presence of any size air pocket changes the dynamics of the system and changes the flow characteristics including velocity, pressure, and compressibility [Vasconcelos and Wright, 2011].

2.2 Life Cycle of Air Phase in Stormwater Tunnels

There are two general types of air pocket formation related to stormwater systems. Ramezani et al. [2016] presents various ways in which air is introduced into a stormwater

system including water plunging in trop shafts, dissolved air in saturated water, leaky valves, rapid infilling and pump inlets.

When small air bubbles enter into the system, they collect in the high points of the system and combine to form larger air pockets. This process is referred to as air entrainment. Much research has been done on this problem [Chanson, 1996].

Conversely, when large amounts of air become trapped in the system due to events such as rapid filling, this is referred to as air pocket entrapment. Air is initially present in stormwater systems prior to filling process, and in general is displaced by water inflows and released through available ventilation points. Based on experimental observation, when inflow rates are gradual, pressurization interfaces are nearly horizontal and air pocket formation is not observed [Patrick and Vasconcelos, 2015]. However, when rapid inflows are observed, various air pocket formation mechanisms can take place, as demonstrated in experiments by Li and McCorquodale [1999], Vasconcelos and Wright [2006], among others.

Following entrapment, air pockets may move, as detailed in the next section. As pockets move, they may be subject to compression and expansion and at certain locations can be expelled. This expulsion may lead to displacement of water, which in turn can lead to geysering problems.

2.3 Air Pocket Motion

2.3.1 Horizontal Motion of Entrapped Air

As pointed out earlier, once entrapped, air pockets may move within tunnel systems as discrete gravity currents, as described by Baines [1991]. Motion of such pockets is similar to gravity currents, as defined by Benjamin [1968]. The author studied a gravity current as an air cavity of atmospheric pressure which advanced along the upper boundary of a liquid. Benjamin [1968] derived an equation for the maximum velocity of an advancing air pocket when water is allowed to flow freely from the end of the horizontal pipe. He also proposed an argument that an advancing air pocket could not occupy more than half of the pipe diameter

without the motion being stalled. These findings are useful for general design and for the prediction of air-pocket behavior, but there are further questions on their application when considering the behavior of air-pockets when they reach a ventilation point. The pocket celerity will depend on various factors, such as air pocket volumes, existence of background flows, opposition between buoyancy and drag forces, etc. [Chosie et al., 2014]. All of this information can be used when selecting ventilation points because it has been observed in experiments that when an air pocket of significant volume arrives at the base of a water-filled ventilation shaft, these pockets will move vertically [Vasconcelos and Wright, 2011; Lewis and Wright, 2012] and may displace water.

2.3.2 Vertical Two-phase Flows

The rise of gas pockets in vertical liquid columns has been studied in other contexts to some extent, but not as extensively in the context of unsteady stormwater flows. When liquid and gas phases are simultaneously flowing through pipes, it is defined as two phase flow. Various flow patterns can be identified according to the relative flow rate of these phases in closed conduits. The characterization and prediction of the interaction between the two fluid phases is relevant for safety purposes. The most common flow regime classifications are as follows: bubbly, slug, semi-annular, annular, and mist [Morgado et al., 2016], diagrammed in Figure 2.1.

When gas is introduced at a low flow rate into a liquid flow, discrete gas bubbles form throughout the liquid, which is classified as bubbly flow [Shaban and Tavoularis, 2014]. As the flow rate of the gas injection increases, the amount of bubbles increases, causing more collision among the small bubbles. As a result of the collision, larger bubbles are formed, leading to the transition from bubbly flow to slug flow. Slug flow is characterized by large upward moving bubbles occupying most of the cross sectional area of the vertical pipe. These large bubbles, called Taylor bubbles, are shaped like bullets and are separated by regions of bubbly flow [McQuillan and Whalley, 1984]. Liquid from the slug of water above the bubble

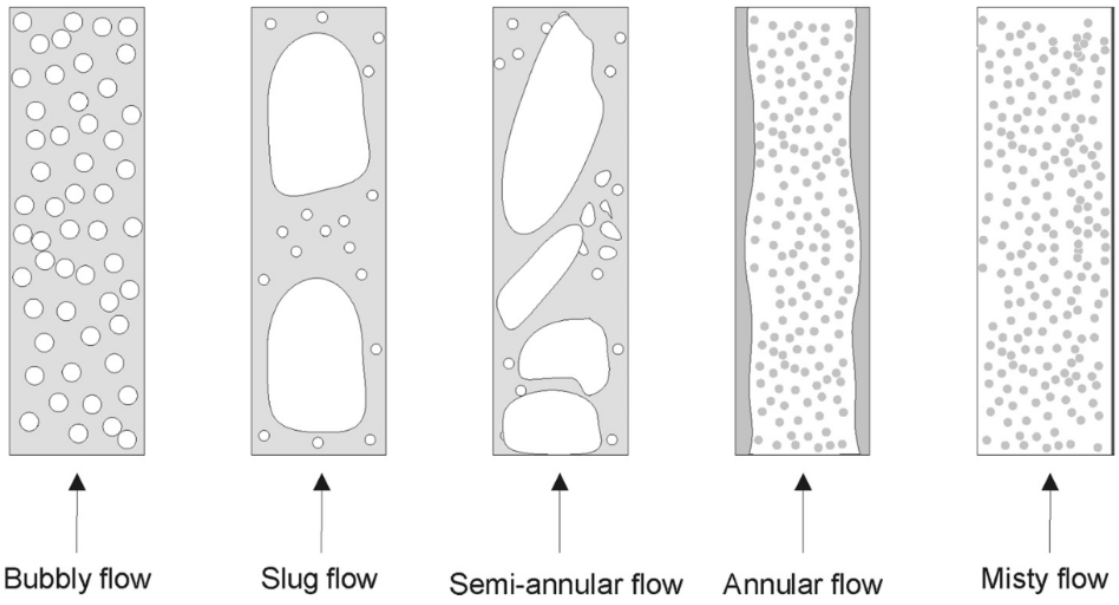

Figure 2.1: Schematic representation of the common gas-liquid flow regimes [Morgado et al., 2016]

falls around the perimeter of the rising bubble, termed film flow. Batchelor [1967] presents a classical problem of the rise of a Taylor bubble. The author pointed that experiments indicate that the steady rising velocity is close to $0.34\sqrt{gD}$, which is consistently below the air pocket rise observations by Vasconcelos and Wright [2011] and Lewis and Wright [2012]. The cause of this is unclear, but may be linked to unsteadiness of air pockets leaving horizontal pipes into vertical pipes, as well the process of air volume increase as it moves in the vertical tower and decompresses. When the film flow around the Taylor bubble accumulates at its trailing edge, the bubbles become divided by short liquid slugs as described by Morgado et al. [2016]. While the gas flow rate continues to increase, the gas phase completely penetrates the liquid slugs, creating a frothy and chaotic flow pattern [Shaban and Tavoularis, 2014], referred to as annular flow. For the highest gas flow rates, the liquid becomes little droplets traveling upward with the gas [Morgado et al., 2016].

These classifications are related to a constant gas injection at the base of the vertical shaft in conditions with steady boundary conditions. However, the research presented in this study deals with single injection air pockets in unsteady conditions. The most relevant

flow regimes to this study are slug flow and annular flow. The air pocket enters the vertical shaft as a large bubble, which would be classified as slug flow. As it travels up the shaft and the film flow accumulates behind the bubble, a wake is created resembling annular flow. Because there is not another gas injection, the remaining water in the vertical shaft becomes annular flow as the gas bubble disperse. In some cases, the mist regime occurs after the slug of water above the air pocket is ejected from the vertical shaft.

2.4 Uncontrolled Air Pocket Release in Stormwater Systems

Vertical air pocket motion may create displacement of water ahead of the pocket, which in turn can lead to discharges of a mix of air and water from the top of these towers. This uncontrolled air pocket release phenomenon is referred to as stormwater geyser, often characterized by jets of air-water mix rising through manholes and other vertical structures. Geyser occurrence may create highly explosive discharges of poor quality conveyed runoff, which can be very damaging and result in a number of deleterious impacts. While relevant, research towards better understanding this phenomenon and implementing mitigation techniques is still limited. Designers for stormwater systems do not have enough guidelines to conceive drop shaft designs that are safe against the impacts of uncontrolled air pocket release.

An initial investigation on the phenomenon of geysers was presented by Guo and Song [1991], who were among the first to observe that intense rain events led the rapid filling of the TARP system in Chicago, which in turn created geysers. The mechanism presented by the authors did not consider the possibility of two-phase flows, so geysering would be a result of mass oscillation processes within tunnel reaches. While a feasible mechanism, Wright et al [2011] pointed out that this mechanism would not be consistent with some of the geysering episodes that have been observed, which are characterized by large discharges of air. In this same work, Wright et al [2011] presented field measurements of an actual geysering episode recorded in Minnesota. While geysers were reported, piezometric pressure heads have not exceeded grade elevation. This is an important and troublesome characteristic of geysering

phenomena since it indicates that even if surge levels do not exceed grade elevation geysers may occur.

Another interesting experimental study related to the release of air phases in vertical pipes was presented by Guedes de Carvalho et al. [2000]. The authors describe flood instability as a phenomenon created when liquid film flow moving downward in the vertical pipes has its interface roughed by a central upward gas flow. As this counter current flow increases, the gas-liquid interface may show waves and liquid detaches from the downward flow and travels upward with the gas pocket. They consequently found that this caused a steep increase in the pressure gradient along the gas pocket. The authors proposed a scaling law relating the onset of flooding instability with the density of the gas phase rising in vertical tubes. It was shown that slugs of air with larger density rising in vertical pipes can have an earlier onset of flooding instabilities when compared to conditions where air is in atmospheric pressure. It is possible that the shearing process created by flooding instability could explain some of the spray characteristics of stormwater geyser releases, however this possibility has not been explored as of today.

Other contributions to the understanding of geysering processes have occurred with respect to the numerical modeling of these episodes. The work by Guo and Song [1991] was possibly the first one that attempted to describe the geysering phenomenon, albeit in a single-phase discharge conditions. Alternative approaches were proposed that consider the case of the water displacement caused by the rise of an air slug. A model based on lumped inertia analysis was presented in Vasconcelos and Wright [2011] and further developed by Lewis and Wright [2012] for the case when the air release occurs amid sustained water pressure in the system. The models were successful in representing the experimental conditions presented by the authors, but failed in attempting the describe the severity of actual geysering episodes.

Shao [2013] developed a 2-D CFD model that used the volume of fluid to compute geysers. It was determined that small pockets do not create large displacements, whereas larger air pockets create large displacements of water and significant air phase flows upon pocket

breakthrough. Another study that has implemented CFD to study geysers was presented by Choi et al [2014], which applied results by Vasconcelos and Wright [2011] to describe the characteristics of geysers created by the release of air pockets in laboratory conditions. The model was able to qualitatively represent some of the measured flow features during the experimental geysering episodes. However, large-scale conditions of actual geysering events pose other modeling challenges (e.g. air phase compressibility) that were not explored in either one of these CFD investigations. An interesting study by Catano-Lopera et al. [2014] involved the use of CFD models to simulate operational issues with the TARP system in Chicago. However, there was not an attempt in that work to systematically evaluate flow conditions related to uncontrolled air releases for geometry parameters, initial water levels and varying entrapped air pocket releases.

2.5 Knowledge Gaps

In summary, geysers are a relevant operational issue that may impact the operation of stormwater systems, but are still not fully understood. Experiments have been performed to evaluate these conditions and some of these investigations have provided relevant insights on this issue. There are difficulties in scaling these experiments considering both air and water phases, so large-scale experiments should be able to offer more details on this phenomenon, as well as support the development of models. Current multiphase flow literature does not discuss the unsteady conditions linked to uncontrolled release of air from pressurized systems. Model developments have been limited, and included simple, lumped inertia approaches as well more complex alternatives using CFD tools. However, these models have not been calibrated with larger scale experimental data, and have not been applied in larger scales that are similar to conditions in actual stormwater systems. This work attempts to address some of these knowledge gaps that have thus far been identified.

Chapter 3

Objectives

This work presents results of experimental and numerical investigations on the geysering created by the release of air pockets of finite volume from stormwater systems in pressurized flow conditions. The work has two specific objectives: 1) to perform observations of these events in large-scale experiments on air pocket release, along with data collection; and 2) to supply experimental results for the calibration of a CFD modeling tool that describes the essential features of a geysering event. The methodology for experimental and numerical investigation is presented next, followed by a section presenting and discussing results of this research, and finally conclusions and recommendations for future work.

Chapter 4

Methodology

4.1 Experimental Apparatus

The experimental apparatus was a scale model of a portion of a stormwater storage tunnel, shown in Figure 4.1. The apparatus included a 13.7-m long clear PVC pipeline, with diameter D_t equal to 302-mm. This near-horizontal pipeline has two reservoirs (volume 1.1 -m^3) supported by wooden structures connected to both the upstream and downstream ends, and were used to sustain pressures in the system during the air pocket releases. About 10.7-m from the upstream point of the horizontal pipeline there was a tee connection, in which vertical shafts (4.7-4.9 m long) of varying diameters (102-mm, 153-mm and 202-mm) were installed. Most of the experiments involved water in quiescent conditions, with a few cases performed with background flows.

Attached near the upstream end of the 302-mm horizontal apparatus, there was a 6-m long, 202-mm diameter clear PVC spur pipeline that served as an air chamber to store a known volume of air. This air phase was set at preselected pressures values that were represented the same pressures in the water side of the apparatus prior to the air pocket release. Halfway within this air chamber, a knife gate valve allowed for volume of air V of either 100 or 200-L to be stored prior to release.

In order to characterize the release of the air pocket, the following instruments were used:

- Three piezo-resistive pressure transducers (one MEGGITT-ENDEVCO 8510C-50 rated at 0.34-MPa, and two MEGGITT-ENDEVCO 8510C-15 rated at 0.103- MPa), shown

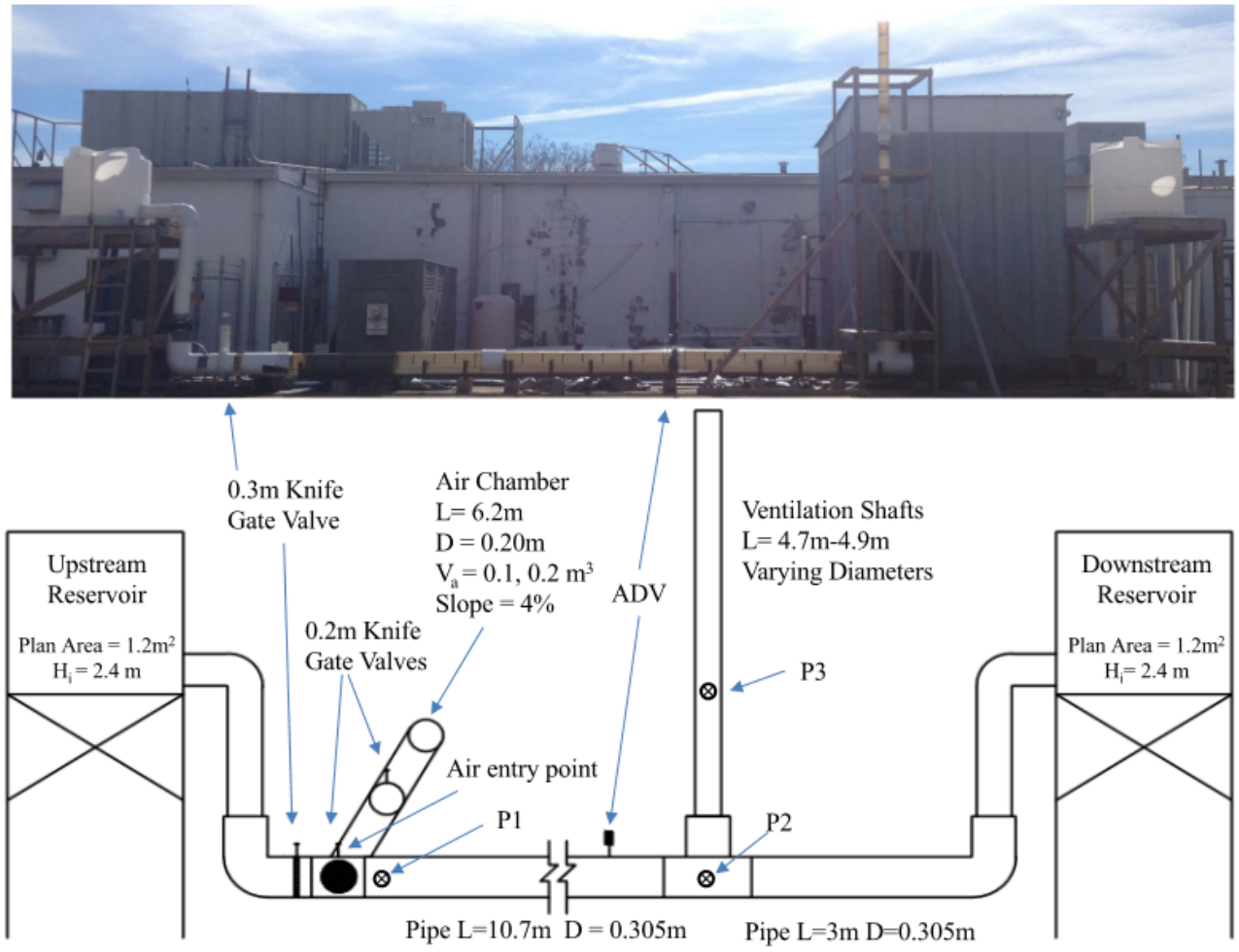

Figure 4.1: Top: Picture of apparatus used in experiments. Bottom: Sketch of apparatus used in experiments.

in Figure 4.2, installed at 0.6-m and 9-m from the upstream end of the horizontal pipeline and one 1.2-m up the vertical shaft (Figure 4.2);

- National Instruments NI-USB6210 data acquisition board sampling pressures at a frequency of 200-Hz (Figure 4.3);
- Two Extech HD750 differential pressure manometers (Figure 4.4), one immediately downstream from the air chamber and the other at the base of the vertical shaft(Figure 4.4);
- Vectrino Acoustic Doppler Velocimeter (ADV) sampling at 25-Hz located 7.5-m downstream from the isolation valve, (Figure 4.5);
- Digital HD camcorder, recording the advance if the air-water interface at 30 frames per second;

Figure 4.2: one MEGGITT-ENDEVCO 8510C-50 rated at 0.34-MPa, and two MEGGITT-ENDEVCO 8510C-15 rated at 0.103- MPa

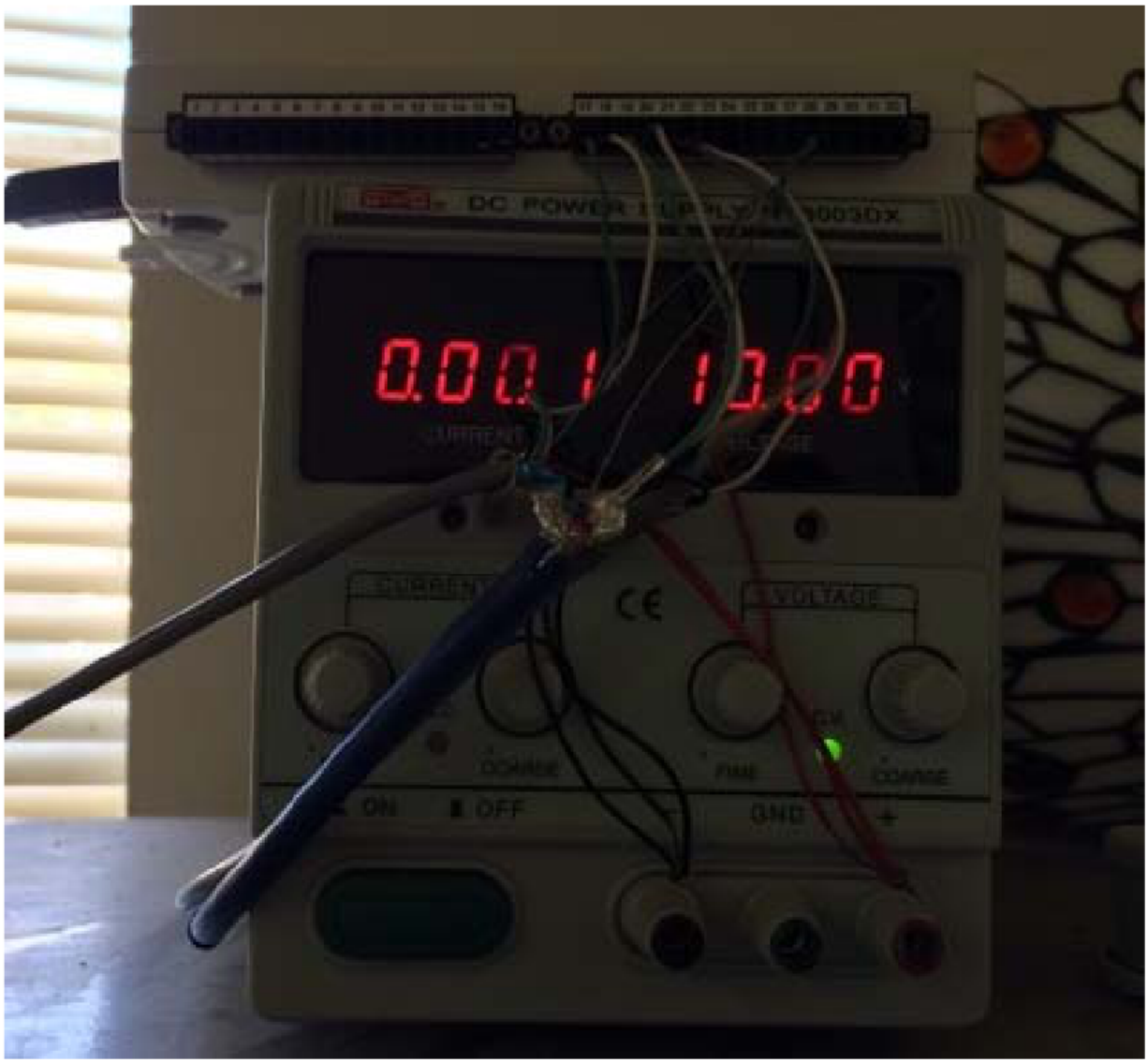

Figure 4.3: National Instruments NI-USB6210 data acquisition board

Figure 4.4: Extech HD750 differential pressure manometer

Figure 4.5: Vectrino Acoustic Doppler Velocimeter (ADV)

4.2 Experimental Procedure

A brief description of the experimental run is as follows. Initially the apparatus was filled with water to a intermediate level within the vertical shaft. A known air volume in the air chamber was pressurized to a level that was similar to the one observed in the vertical shaft. Upon the opening of the knife-gate valve linking the air chamber to the water-filled horizontal pipe, the air pocket was released and advanced in the horizontal pipeline until it reached the base of the vertical shaft. Water levels in the shaft varied during the rise of the air pocket, as described by Vasconcelos and Wright [2011], and in various cases the level reached the upper end of the shaft, characterizing a geyser event. A 302-mm knife gate valve at the upstream end of the horizontal pipeline (302-mm) was partially closed during experiments. This prevented the released air from returning to the upstream water reservoir.

The experimental procedure was performed as follows:

1. With the air chamber knife gate valve closed, the apparatus was filled with water to a piezometric head about 2.7-m with respect to the horizontal pipe invert;

2. Water was in quiescent conditions prior to air release. In the cases that background flows were used, recirculation pumps created a water velocity of about 0.25-m/s in the pipe;

3. The air compressor was turned on and the air pressure in the chamber was adjusted to approximately match the water pressure within the horizontal pipe in an attempt to reduce the amplitude of inertial oscillations in the ventilation tower upon opening the air chamber valve;

4. Data collection from the pressure transducers, ADV, and video camera was started and the initial manometer readings were recorded;

5. The gate valve to the air chamber was quickly opened (around 0.5 second) with one swift motion to allow the sudden release of the air pocket;

6. Upon release, the entrapped air pocket advanced in the system toward the vertical shaft similarly to a cavity described by Baines [1991] and Chosie et al. [2014];

7. After about 10 seconds, the air pocket arrived at the base of the vertical shaft, causing the displacement of the water present in the shaft;

8. After steady state was reached, final pressure measurements were recorded with manometers and all data recording devices were turned off.

4.3 Experimental Variables

Two main experimental variables were used in the proposed experiments: the ventilation shaft diameters and the volume of air pockets released. Three diameter values were used: $D^* = 0.33, 0.50$ and 0.67 (ranging from 102-mm to 202-mm). Two air pocket volumes were used: $V^*_{air} = 3.5$ and 7.0 (100 L and 200 L). Some experiments were performed with background flows (creating velocities around 0.25 m/s) Most experimental conditions were repeated at least three times in order to ensure consistency of the experimental results.

Table 4.1 outlines the combinations of variables that were tested in this study.

Table 4.1: Tested Conditions

Tunnel dimension D_t (m)	Shaft diameter D (m)	D*= D/D_t	V_{air} (L)	V_{air}*= V_{air}/D_t^3	Background flows (y/n)
0.30	0.10	0.33	100	3.5	No
0.30	0.10	0.33	100	3.5	Yes
0.30	0.10	0.33	200	7.0	No
0.30	0.10	0.33	200	7.0	Yes
0.30	0.15	0.50	100	3.5	No
0.30	0.15	0.50	100	3.5	Yes
0.30	0.15	0.50	200	7.0	No
0.30	0.15	0.50	200	7.0	Yes
0.30	0.20	0.67	100	3.5	No
0.30	0.20	0.67	100	3.5	Yes
0.30	0.20	0.67	200	7.0	No
0.30	0.20	0.67	200	7.0	Yes

4.4 Procedure for Data Analysis

Once the experimental runs were complete, the data analysis process was initiated. Videos were downloaded and visually analyzed to determine the vertical displacement of both the air pocket (air-water interface, or Y_{Int}) and the free surface of the water within the vertical shaft (referred to as Y_{FS}). This was done by progressing frame by frame through the videos and noting the time at which each surface reached the marks on the vertical shaft at 0.30-m intervals. Then this data was used to calculate the velocity associated with Y_{Int} and Y_{FS} motion by dividing the distance traveled over elapsed times.

Values for vertical displacements and velocities, air pocket volume and vertical tower diameters were normalized, and starred variables * refer to the normalized versions of the variables. Vertical displacement measurements were normalized by the length of the vertical shaft L (Equations 4.1 and 4.2). Velocities of the free surface V_{FS} or the vertical air-water interfaces V_{Int} were normalized by $\sqrt{gD}$ (Equations 4.3 and 4.4). Air pocket volumes V_{air} were normalized by D_t^3 (Equation 4.5), whereas vertical tower diameters D were normalized by the horizontal pipe diameter D_t (Equation 4.6).

$$Y^*_{FS} = Y_{FS}/L \tag{4.1}$$

$$Y^*_{Int} = Y_{Int}/L \tag{4.2}$$

$$V^*_{FS} = V_{FS}/\sqrt{gD} \tag{4.3}$$

$$V^*_{Int} = V_{Int}/\sqrt{gD} \tag{4.4}$$

$$V^*_{air} = V_{air}/D_t^3 \tag{4.5}$$

$$D^* = D/D_t \tag{4.6}$$

The testing conditions presented in this study included three vertical shaft diameters and two air pocket volumes. The three ventilation shaft diameters used were D*=0.33, 0.50 and 0.67, with air-pocket volumes V*= 3.5 and 7.0, with and without the presence of background flows. Most experimental conditions were repeated three times in order to ensure consistency of the experimental results.

Pressure transducer data was sampled at 200 Hz frequency. This voltage data was then converted into pressure head readings based on the linear relationship between voltage and pressure. The initial and final pressure head values, measured with an accuracy of 0.01 m, were used for calibration. Considering the 3% error associated with the pressure transducers, the accuracy of the pressure head readings at the base of the tower and the air-inlet junction are 0.03 m and the accuracy of the pressure head readings in the tower are 0.10m.

Chapter 5

Results and analysis

5.1 Kinematics

As pointed out earlier in the experimental procedure, the tests begin with an initial water level of about 2 m in the vertical shaft, measured from the base of the visible vertical tower. The opening of the 202-mm knife gate valve released the air pocket into the system. Even though the air pressure matched the initial water piezometric pressure in the apparatus, a few inertial oscillations were observed on the shaft upon the valve opening, which lasted few seconds. The air pocket travels in the horizontal tunnel toward the vertical shaft with a celerity of around 0.9-m/s. By the time when the pocket arrived near the base of vertical shaft, the inertial oscillations were not significant.

5.1.1 Displacement of Air and Water within the Vertical Shaft

In most of the tested cases the water displacement exceeded 2.7 m, which led to geysering through the top of the shaft. It is important to state that the geysering criteria used in this study is based on the release of a slug of water ahead of the rising air pocket rather than the splash of water created in the tower during the release, which is used by some other studies. However, the releases were characterized by a significant mix of air and water, many times with an explosive nature. In a few of the tested cases there was more than one discharge of water through the top of the shaft. Following the air-water discharge, a complex flow pattern with smaller slugs and bubbles rising was observed in the vertical tower which lasted for a few seconds. The water level at the top of the shaft also presented inertial oscillations following the air discharge for various seconds afterwards.

The vertical trajectory of the air pocket interface and the free surface as they travel up the vertical shaft is presented in Figure 5.1. All test runs are presented for each combination of pocket volume and vertical shaft diameter with no background flows. The error related to both the time ($\approx 0.03\,s$) and the vertical coordinate measurements ($\approx 0.08\,m$) are small and not represented on the figure. All cases showed a rise of both air-water interface and free surface, and the curved trajectories observed for $D^* = 0.33$ and $D^* = 0.50$ indicate that both free surface and interface velocities increased over time. However, for the single case were geysers were not reported ($D^* = 0.67, V^*_{air} = 3.5$) the free surface level achieved a maximum elevation and receded prior to the breakthrough of the air pocket (Y_{FS}=Y_{Int}). This type of outcome in air pocket release processes has not been reported in earlier related investigations and indicate that the trajectory of water is not always monotonic.

When compared to normalized displacement results presented by Vasconcelos and Wright [2011], the results presented in this study vary when considering the acceleration of both the leading edge of the air pocket (air-water interface, or interface) and the surface of the water in the shaft that is open to the atmosphere (free surface). As shown in Figure 5.2, the trajectory of both free surface and air-water interfaces are curved, whereas comparable results presented by Vasconcelos and Wright [2011] indicated linear trajectories. This is attributed to the current experimental apparatus sustaining pressures during air release, unlike the work by Vasconcelos and Wright [2011]. Expansion of the air pocket during the release process may also account for this curved trajectory of the free surface and air-water interface. A difference between the present findings and the results from Wright [2013] is related to the normalized pocket size after which the normalized height at which the air pocket breaks through the free surface becomes constant. The previous study by Wright [2013] pointed out that this volume is $V^*_{air} \approx 4$. The present measurements, however, indicate significant differences in the outcome of the pocket volume release of $V^*_{air} = 7$ through a $D^* = 0.67$ shaft, whereas a $V^*_{air} \approx 3.5$ in same conditions did not resulted in a geyser.

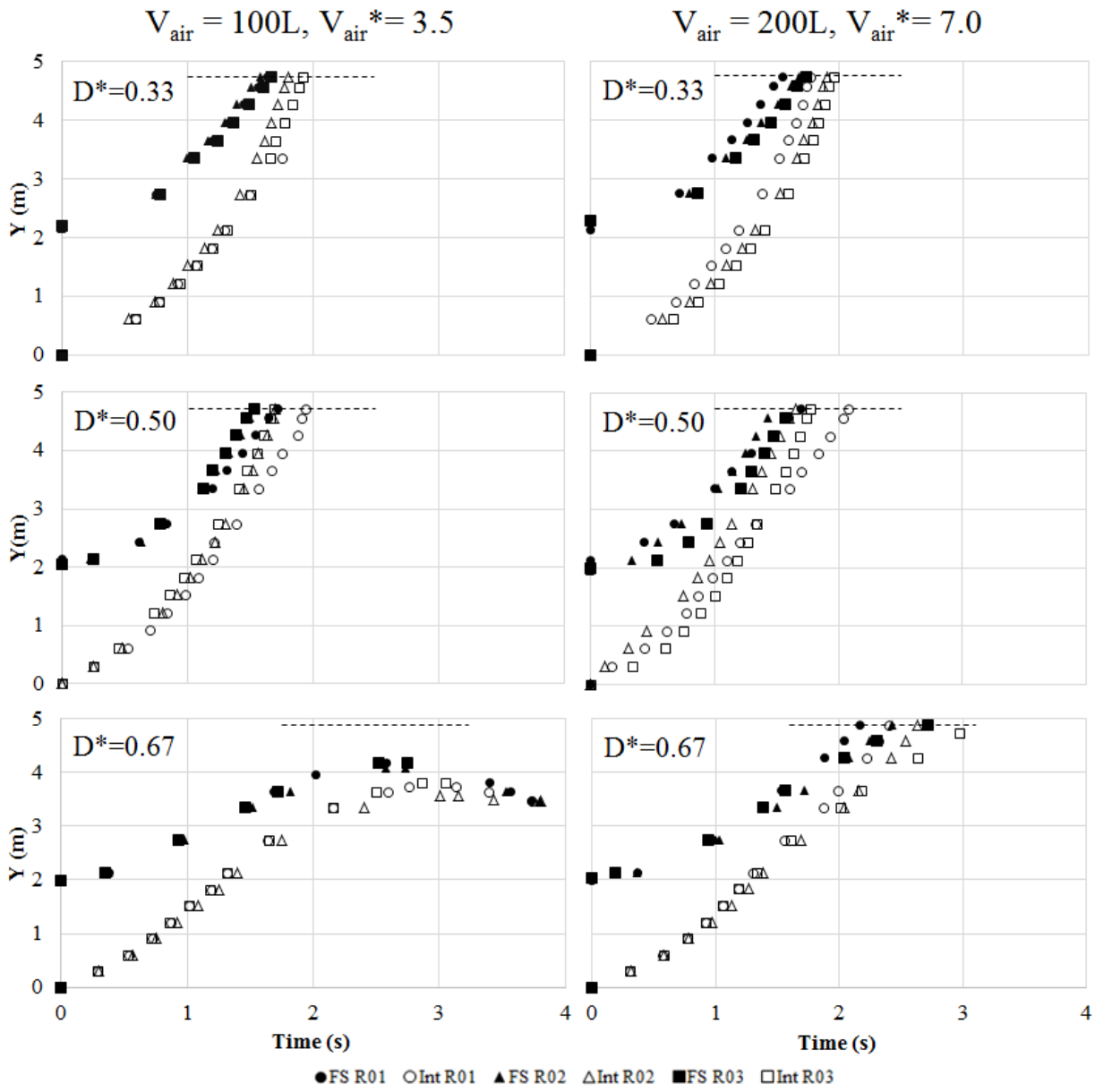

Figure 5.1: Vertical displacement of the free surface (FS) and the air-water interface (Int): Time evolution of free surface and interface coordinates including all test runs (R01, R02, R03) for every tested condition without background flows. The filled-in symbols represent the free surface and the open symbols represent the air-water interface coordinates. Diameters of 0.10, 0.15, and 0.20 m were normalized by the diameter of the horizontal tunnel, 0.30-m. The elevation of the rim of the vertical shaft is indicated by the dashed line.

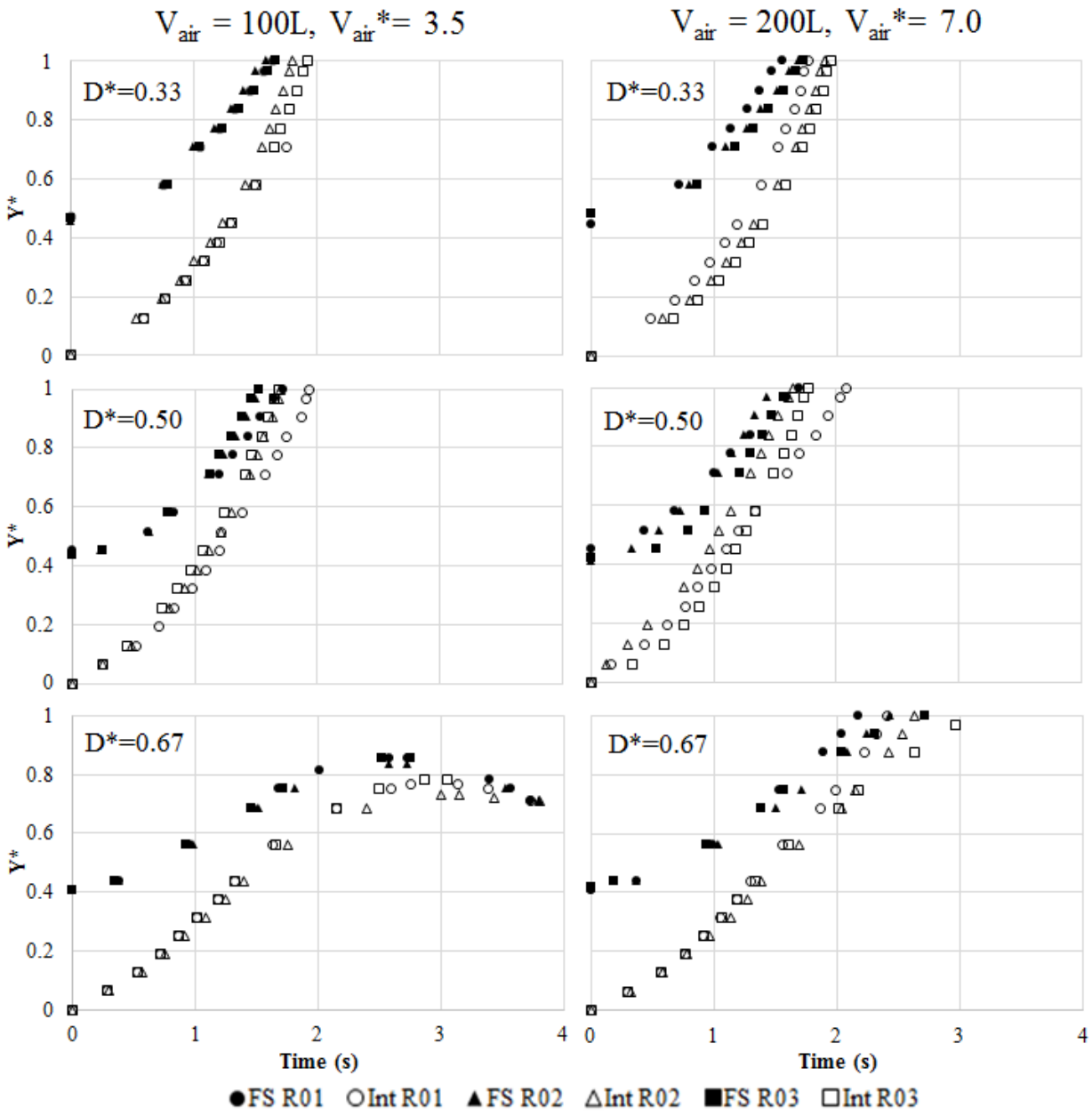

Figure 5.2: Normalized displacement of the free surface and the air-water interface: Time evolution of free surface and interface coordinates including all test runs (R01, R02, R03) for every tested condition without background flows. The filled-in symbols represent the free surface (FS) and the open symbols represent the air-water interface (Int) coordinates. Diameters of 0.10, 0.15, and 0.20 m were normalized by the diameter of the horizontal tunnel, 0.30-m. The elevation of the rim is represented by the Y* value of 1.

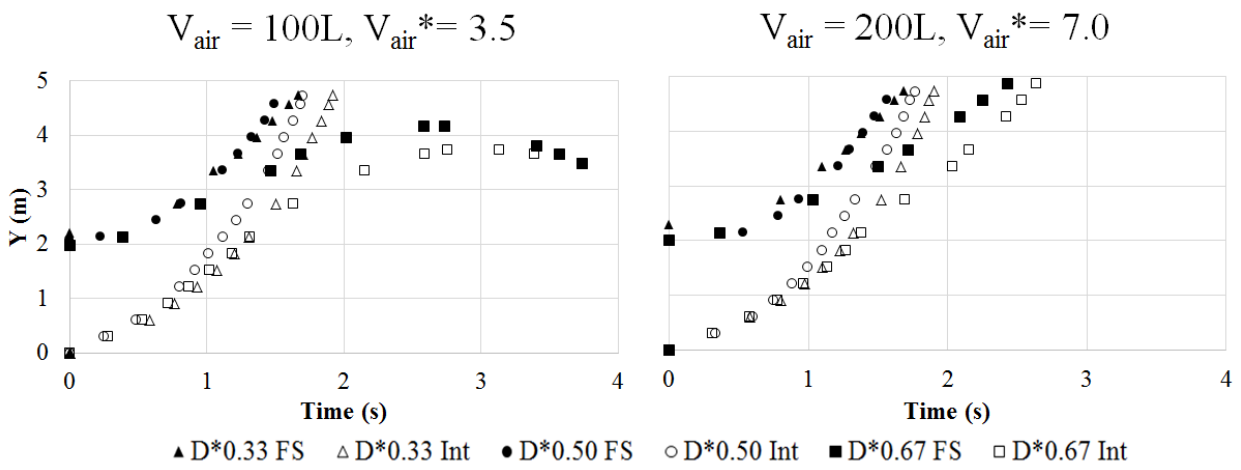

Figure 5.3: Effect of varying diameters in Y_{FS} and Y_{Int} variation over time, in the absence of background flows (only one repetition for each diameteris presented).

Figure 5.3, which compares the displacement over time among different diameters for both air pocket volumes, indicates that for the D^*=0.33 and D^*=0.50 shafts there is not a major difference between the progressions of the free surface up the vertical shaft. However, for both air pocket volumes, the pocket initially travels up the D^*=0.50 shaft at approximately the same rate until it reaches 1-m. At this point, the pocket in the D^*=0.50 shaft begins to move more quickly, and reaches the top of the shaft in slightly less time than the pocket in the D^*=0.33 shaft. This may be caused by a larger imbalance between the downward film flow rate and the displaced volume created by the air pocket rising in the D^*=0.50 shaft. Based on the continuity of the air phase vertical flow [Vasconcelos and Wright, 2011], if the film flow rate was larger, the free surface would progress more slowly and it would take more time for the air pocket to reach the rim of the shaft. Figure 5.3 also reveals that the behavior of the air pocket is changed in the largest tested diameter, rising noticeable more slowly than the air pockets in the smaller shafts.

When compared to normalized displacement results presented by Vasconcelos and Wright [2011], the results presented in this study vary in terms of the acceleration of both the air pocket and the free surface. As shown in Figure 5.2, when considering only the conditions

that produced a geyser, the data from this study shows a more parabolic trend whereas the results presented by Vasconcelos and Wright [2011] show a more linear trajectory of both air and water, with the free surface and the air-water interface meeting before they reach the top of the vertical shaft. Even when considering the single case where a geyser does not occur, the trajectory does not follow this trend. This contradiction can most likely be attributed to the lack of a reservoir to maintain the pressures in the Vasconcelos and Wright [2011] study.

For all tested cases, the displacement of the free surface, ΔY_{FS}, reached or exceeded 2.0 m, with most of the cases displacing more than 2.7 m, as seen in Figure 5.1. When this assumed free surface displacement is normalized by the tunnel diameter, $\Delta Y_{FS}/D_t$, the result is 9 for all cases that resulted in geysers. These results are in general smaller than the ones presented in Wright [2013]. This could be linked to the difference in air pressure head between this work (≈2.7 m) and the previous work (≈0.5 m). An important result from these study is that even with $D^* = 0.67$ there was a significant amount of water displaced. One major difference to be observed between these two works is the effects of the air pocket size on the displacement. Wright [2013] states that after a certain normalized pocket size (V*≈4) the height at which the air pocket breaks through the free surface becomes constant when normalized by the tunnel diameter and approaches a value of about 12. However, the results in the study do not fully support this conclusion. For example, consider the bottom row of Figure 5.1 showing the displacement results for the $D^* = 0.67$ shaft. The left graph is for the $V^*_{air} = 3.5$ air pocket and the right graph is for the $V^*_{air} = 7.0$ case. As shown, for the smaller air pocket, the amount of water displaced is about 2 m before the air pocket breaks through the free surface, making the normalized displacement about 6.67. When compared with the results for the $V^*_{air} = 7.0$ air pocket, with a normalized free surface displacement of at least 9, limiting the application of Wright's conclusion the $V^*_{air} = 4$ is the limiting value for air pocket displacement.

Discussion on the effects of background flows on displacement can be found in the following sections.

5.1.2 Velocity

The velocity results for the air-water interface and free surface were calculated from the measured displacement of the flow features, and are presented in Figure 5.4. These results indicate a slight decrease between $D^* = 0.33$ and $D^* = 0.50$, with the exception of two data points from two different runs, and a more pronounced velocity drop for $D^* = 0.67$. It was noticed that the velocity for $D^* = 0.67$ and $V^*_{air} = 3.5$ became slightly negative, consistent with the receding free surface interface observed for this condition. In absolute terms, velocity of rising air pockets were higher for the $D^* = 0.50$ condition, slightly more than $D^* = 0.33$, a result that was not previously reported in related studies. The velocity results do not present a steady behavior, but rather present a "wobbling" pattern, which may be linked to compression and decompression of the air pocket as it moved upward. A more pronounced wobbling effect was also presented in Vasconcelos and Wright [2011]. Additionally, much faster growth of the air-water interface velocity is noticed when geysering initiates. It is assumed that once the water is discharged at the top of the vertical shaft there is a further increase in the pressure gradient experienced in the air phase, leading to even faster upward motion.

The normalized velocity results for the air-water interface and free surface were calculated by dividing the calculated velocity by $\sqrt{gD}$, and are presented in Figure 5.5. Compared to results presented by Vasconcelos and Wright [2011], these results are 3-4 times higher for larger diameter shaft ($D^* = 0.607$), with normalized velocities averaging in the range of 0.25-0.5. For the smaller diameter shafts presented, the normalized velocity increased similarly to the ones in the current study. This can possibly be attributed to the reservoirs in the current experiment that maintained the pressure in the system during geyser occurrence.

5.1.3 Background Flows

Experiments were also performed with background flows in the horizontal pipe, created by two recirculation pumps that would link the two water reservoirs above the water towers through two 50-mm flexible hoses. The resulting average flow obtained with these two pumps was in the order of 0.20 m/s to 0.30 m/s during typical experiments. The rationale for using recirculation pumps was to create a larger volumetric displacement of the air pocket in the horizontal pipe, under the assumption that this displacement would increase the amount of admitted air in the vertical shafts. Indeed, the celerity of the air pocket leading edge in the horizontal pipe was increased, and the propagation time of the horizontal pocket decreased from 10 seconds to 8 seconds on average.

However, there were no significant changes in the behavior of the air release in the vertical shaft. The added velocity has not influenced the amount of the air that entered the vertical shaft, as the experimental results in the trajectories of the free surface and air-water interfaces within the shaft indicate. By comparing Figures 5.1 and 5.6, it may be noticed that the the case with $D^* = 0.67$ and $V^* = 3.5$ presented larger displacement of the free surface (about 15%) for the case with background flows. However, all other cases were very much similar, both in terms of the trajectories of the free surface and in terms of the velocities of the flow features.

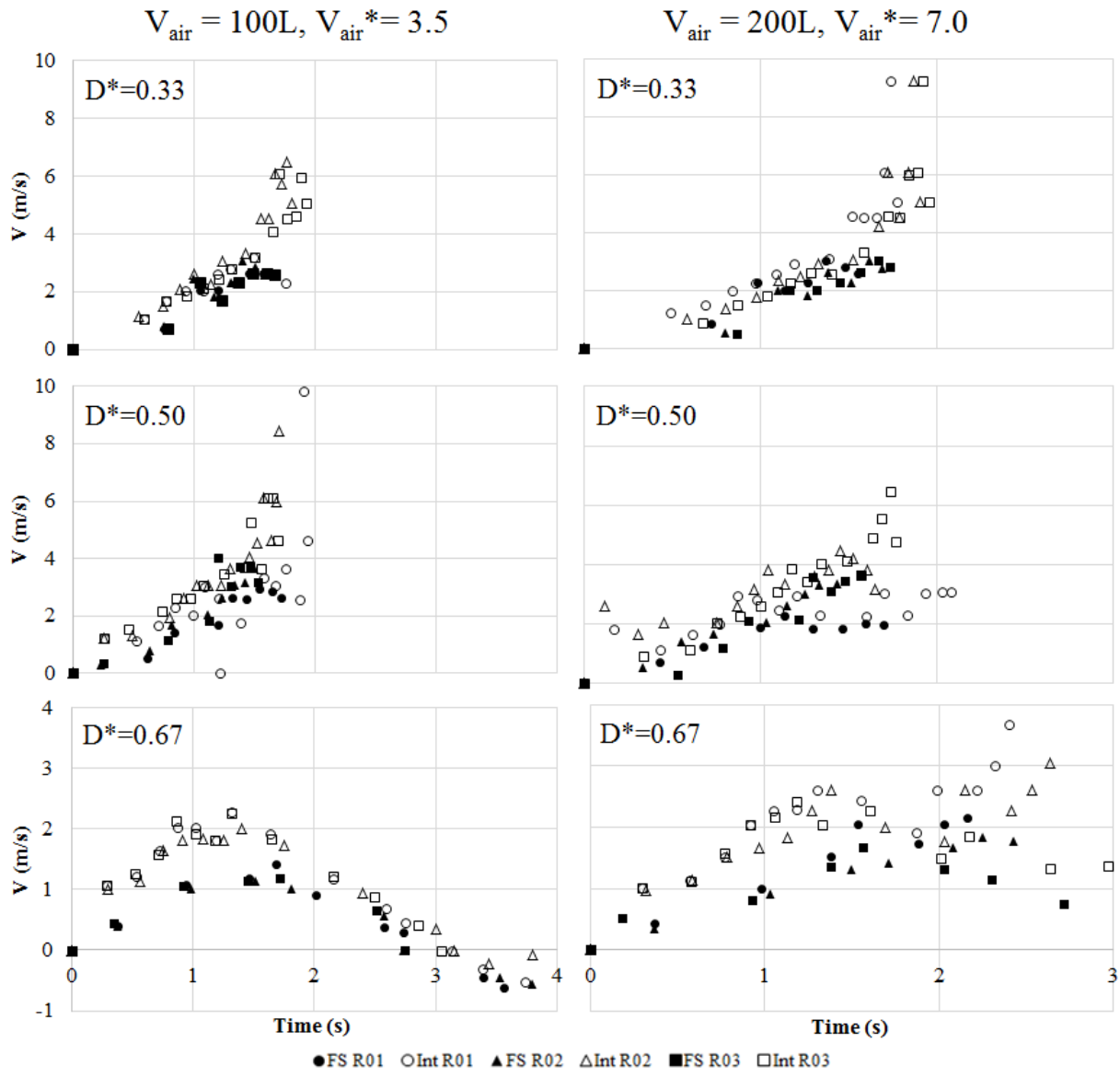

Figure 5.4: Time evolution of the free surface and the air-water interface coordinates including all test runs (R01, R02, R03) for every tested condition without background flows. The filled-in symbols represent the free surface (FS) and the open symbols represent the air-water interface (Int) coordinates.

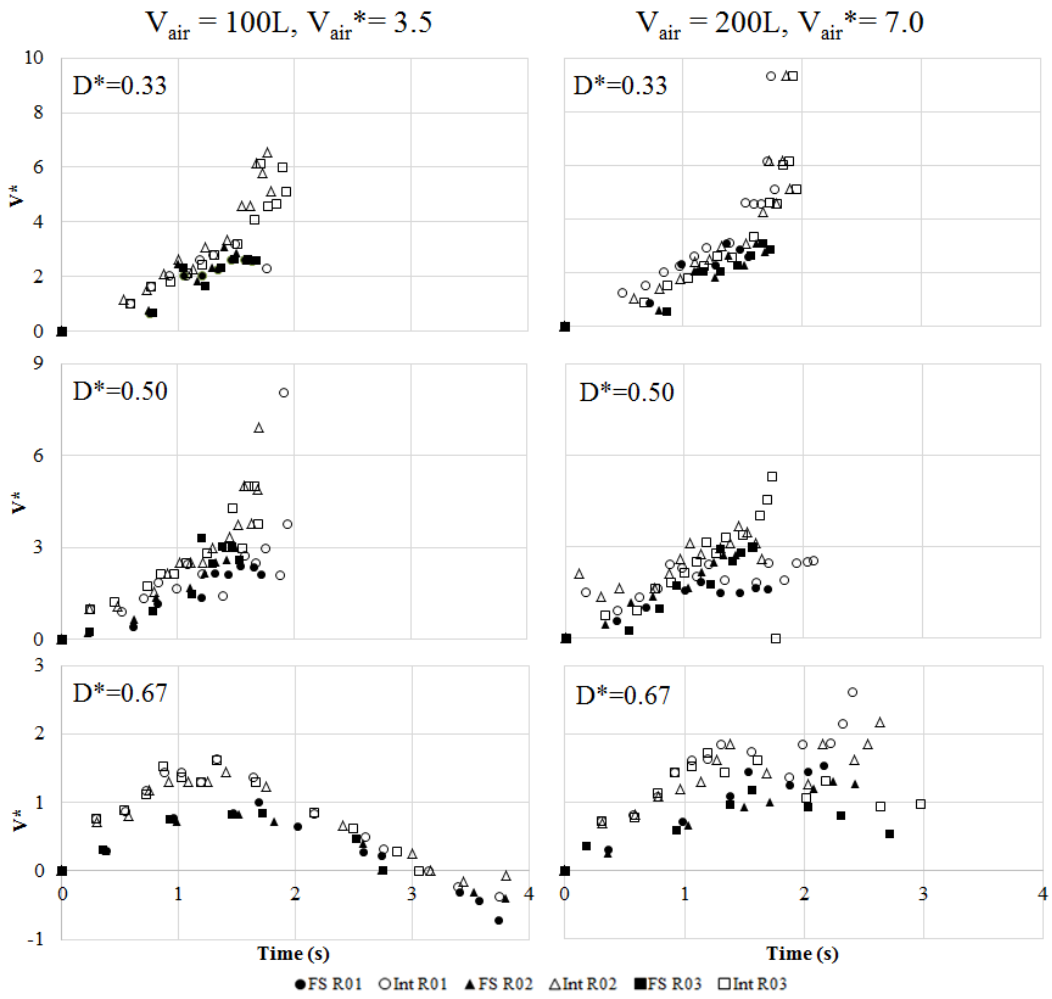

Figure 5.5: Time evolution of the normalized free surface and the air-water interface coordinates including all test runs (R01, R02, R03) for every tested condition without background flows. The filled-in symbols represent the free surface (FS) and the open symbols represent the air-water interface (Int) coordinates.

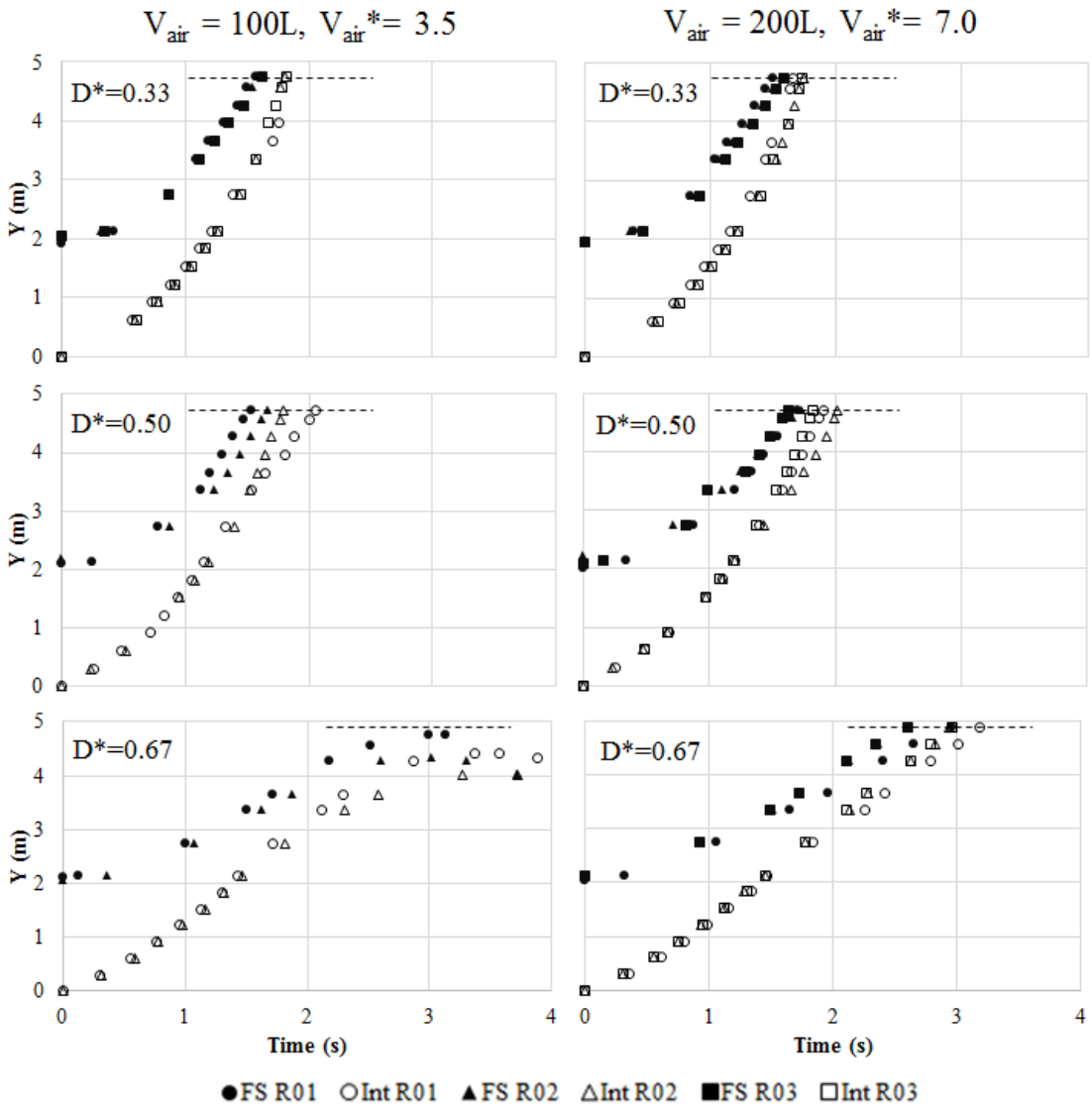

Figure 5.6: Time evolution of the free surface (FS) and the air-water interface (Int) coordinates including all test runs (R01, R02, R03) for every tested condition with background flows. The filled-in symbols represent the free surface and the open symbols represent the air-water interface coordinates.

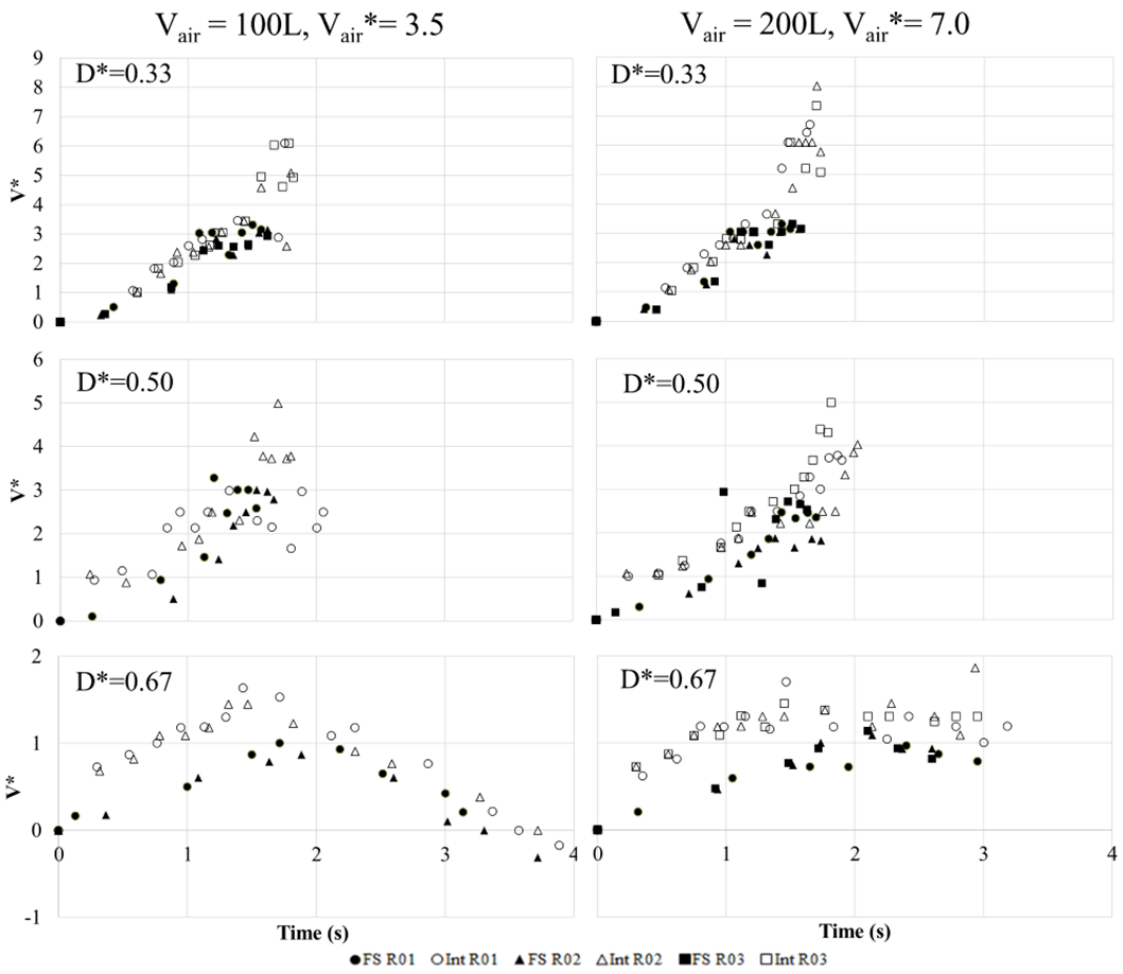

Figure 5.7: Time evolution of the normalized free surface and the air-water interface velocities including all test runs (R01, R02, R03) for every tested condition with background flows. The filled-in symbols represent the free surface (FS) and the open symbols represent the air-water interface (Int) coordinates.

5.2 Pressure Head

Figure 5.8 presents pressure results measured from the moment when the air release occurred for a representative case involving a 202-mm diameter shaft and $V^*_{air} = 7.0$, with pressure recordings at the bottom (P2 transducer) and lateral (P3 transducer) of the vertical shaft. The initial inertial oscillations are observed in Figure 5.8 approximately 10 seconds prior to the instant when the air arrives in the vertical shaft. For that specific condition, this inertial oscillation period (around 3 seconds) is altered when the air reaches the base of the vertical shaft, as pressure results presented more erratic patterns. While the rise of the air pocket and free surface interface over time are in general monotonic, as indicated in Figure 5.1, it is speculated that small changes in air-water interface velocities can lead to fluctuations in pressure recorded in the shaft.

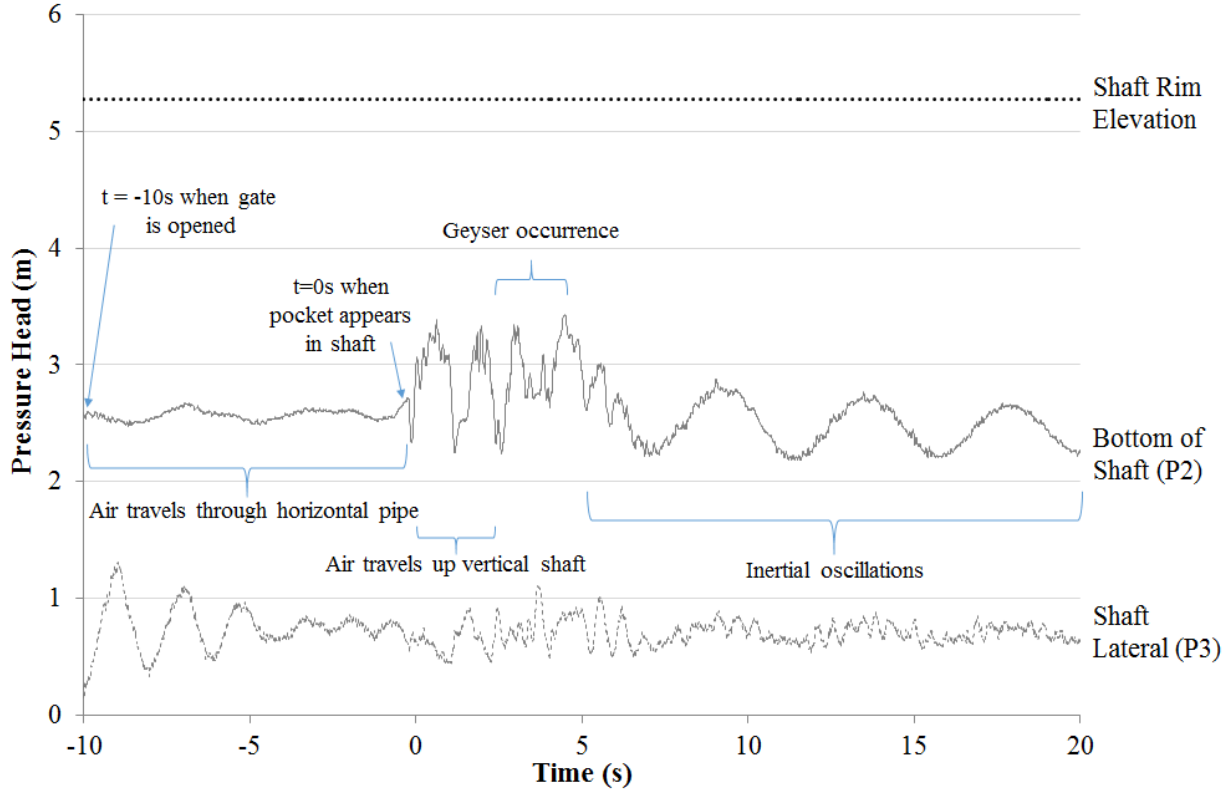

Figure 5.8: Sample pressure head date from a $0.20 - m$ diameter shaft with a $200 - L$ air pocket. Captions indicate the progression of the air pocket.

Large swings in pressure read at the vertical shaft continue during the short period where air-water discharge (geysering) occurred. After the geysering, air continued to migrate upward in the shaft and the complex bubbly flow eventually approached single phase conditions, with more regular mass oscillations at the end of the pressure hydrograph reflecting this final condition as the reservoirs refilled the vertical shaft. Finally, the amplitude of the pressure fluctuation observed in P3 was not as large as P2, and neither of the piezometric pressure head values were large enough to reach the elevation of the vertical shaft rim.

Figure 5.9 presents a set of representative pressure data for the three diameters and both air pocket volumes studied. The data sets were trimmed to display only the data for period during the water upward motion in the vertical shaft. The range of pressure fluctuations was decreased with the shaft diameter D, however the pressures did not exceed levels compatible with the vertical shaft rim in any tested condition. Geysers occurred in all of these cases between 2 and 3 seconds, but no clear trend in the pressure values was identified during these releases. It was noticed that the largest pressure variations were observed in the junction next to the location where the air phase was introduced in the system. Also it was noticed that the largest variations in pressure occurred with the two smaller diameters for the vertical shaft, whereas the cases with D^*=0.67 presented the smallest variation during air release occurrences at the shaft. This points to the benefit of having large-diameter shafts in mitigating pressure fluctuations in tunnel systems following uncontrolled air releases.

Figure 5.10 contains data from "worst-case" tests from each of the shaft diameters with a $V^*_{air} = 7.0$ air-pocket that supports the claim that the pressure heads observed in the system were not sufficient to cause a geyser occurrence without additional forces such as the interaction between air and water.

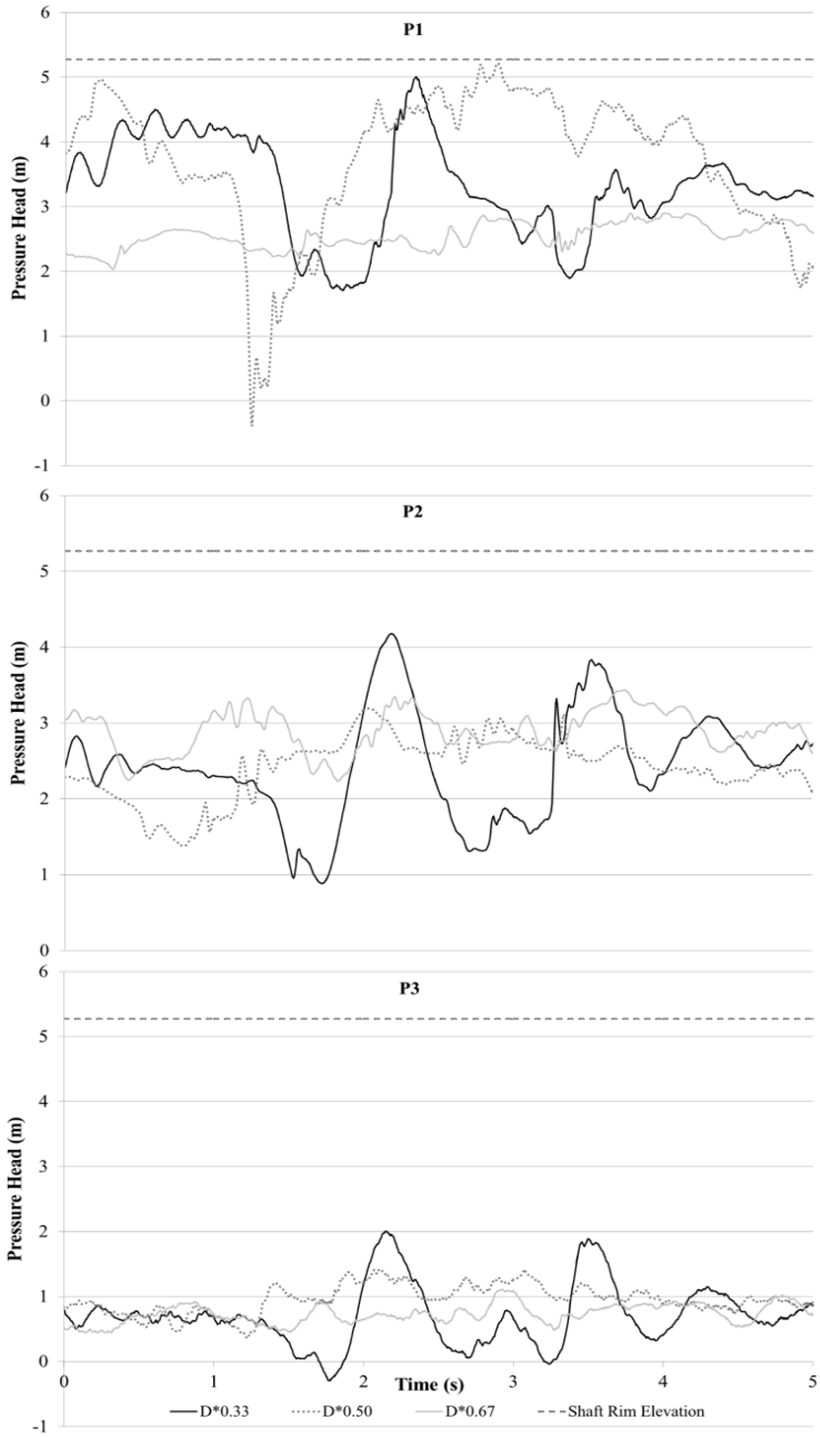

Figure 5.9: Pressure head data from representative test runs of all diameters for the $V_a^* air = 7.0$ air pocket. Top: P1 located at the air inlet, Middle: P2 located at the invert of the horizontal tunnel, Bottom: P3 located on the lateral of the vertical shaft. Time zero corresponds to the time when the air pocket appears in the visible section of the vertical shaft.

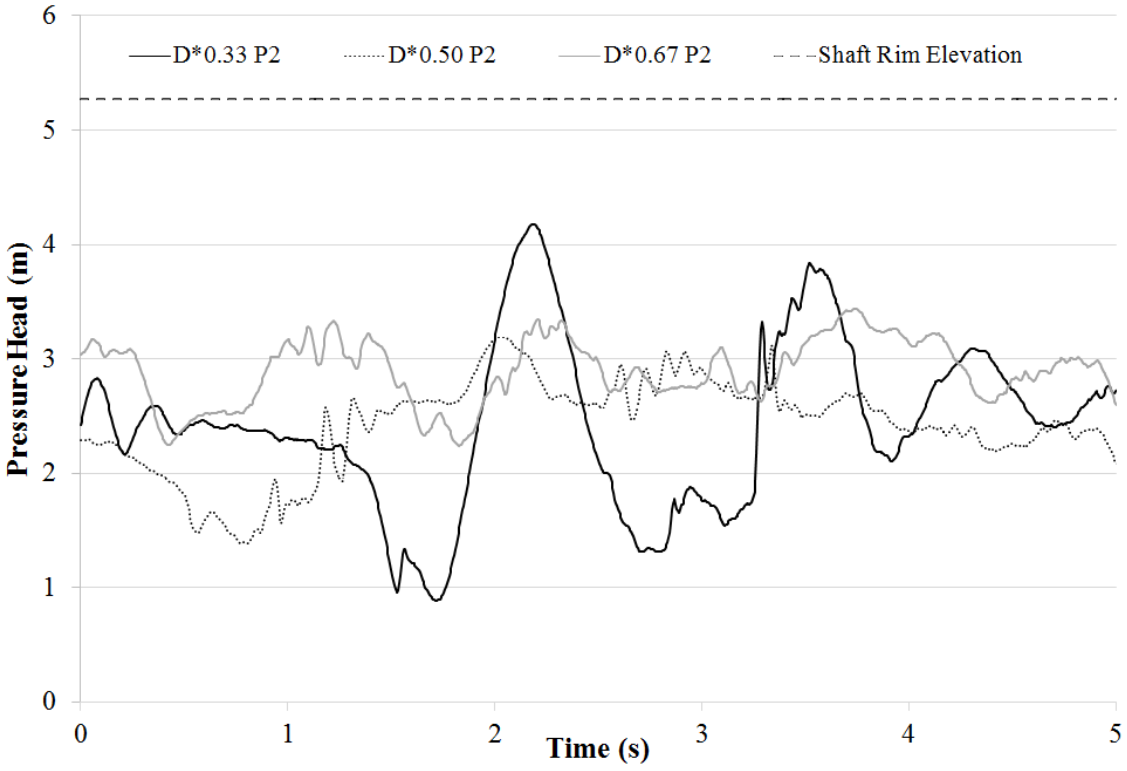

Figure 5.10: Representative pressure head data measured from the bottom of the vertical shaft (P2) including all three shaft diameters with a $200 - L$ air-pocket and without background flows showing that the pressure heads never reach a magnitude large enough to cause a geyser to occur.

5.3 Geyser Series Snapshots

A sequence of photos of the progression of a typical geyser event with relative time stamps is presented in Figure 5.11, where $T_{rel} = 0\,s$ corresponds to the time when the air reached the visible part of the vertical shaft ($Y^*_{Int} = 0$). In the first frame (a), the free surface was about $0.1\,m$ from the rim of the shaft ($Y^* = 0.94$) and the leading edge of the air pocket was about $1\,m$ below at $Y^* = 0.86$. Frame (b) corresponds to the instant where the free surface was at the rim of the shaft, $Y^*_{FS} = 1$ and the air pocket was $0.75\,m$ below ($Y^*_{int} = 0.84$). This frame marks the onset of geyser event considered these investigation. As shown in frame (c), the geysering event progressed as water above the air pocket continued to be expelled like a slug until the air pocket breakthrough to atmosphere ($Y^*_{int} = 1$) about $0.1\,s$ later, as captured in frame (d). While there was no direct measurement of air velocity in these discharges, the CFD-simulated air pocket velocity in frame d is $8.15 m/s$, while in frame (e) is $18.4 m/s$.

Figure 5.11 frames (e) and (f) shows a very complex interaction between the discharged water and the air that is being discharged, which include a fragmentation of the water slug that spread the air pocket several meters in the air. Such air velocities are feasible due to a short-lived, but strong pressure gradient in the tower as soon as air pocket breakthrough and escapes the vertical shaft. While it was not easily observed, it was also noticed a type of 'mist' following the water slug discharge in different tests. It is assumed that flooding instability, such as presented in Guedes de Carvalho et al. [2000], could potentially have occurred between the film flow moving downward along the pipe walls and the air pocket moving upward. As water moved downward during the air release, a fraction of it could have detached and entrained with the upward moving air pocket.

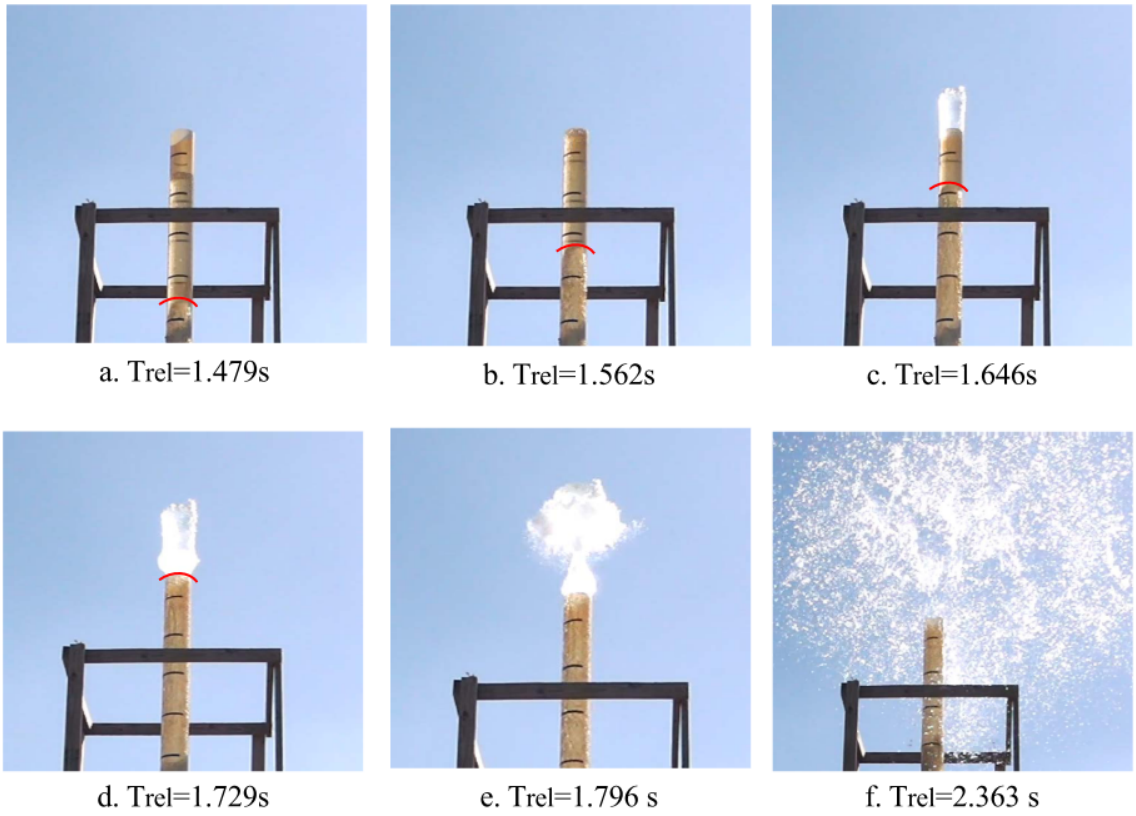

Figure 5.11: Progression of the geysering event from an experiment with a shaft diameter of 0.15-m, a 200-L=a air-pocket and no background flow. The bold line is the artificially exaggerated interface location. Each horizontal line along the pipe is 0.30-m apart. The simulated air pocket velocity when it reaches the top of the tower, shown in frame d, is 8.15-m/s. The simulated velocity after the air exits the shaft is 18.36-m/s

5.4 Results Compared to CFD Model

A CFD model developed by Jue Wang has been applied for all experimental cases, including three vertical shaft diameters and both 100L and 200-L air pockets. In general, the solutions yielded comparatively good agreement with the experimental data, particularly with respect to the simulated displacement of the rising water free surface and air-water interface.

Figure 5.12 presents the comparison of the normalized displacement of the water free surface in the shaft (Y_{FS}) and air-water interface of the rising air pocket (Y_{Int}). Time is referenced to the instant when the air pocket leading edge becomes visible in the vertical

shaft. It can be noticed that the CFD modeling results match the measured data well, considering the natural variability among experimental repetitions. This agreement improved with the discretization, as is noticed comparing results obtained with the coarse mesh with intermediate and fine mesh results. It is noticed that for both CFD and experimental results the air pocket and water column above the pocket rising process ends within 2 seconds, except for the results obtained with the coarse mesh.

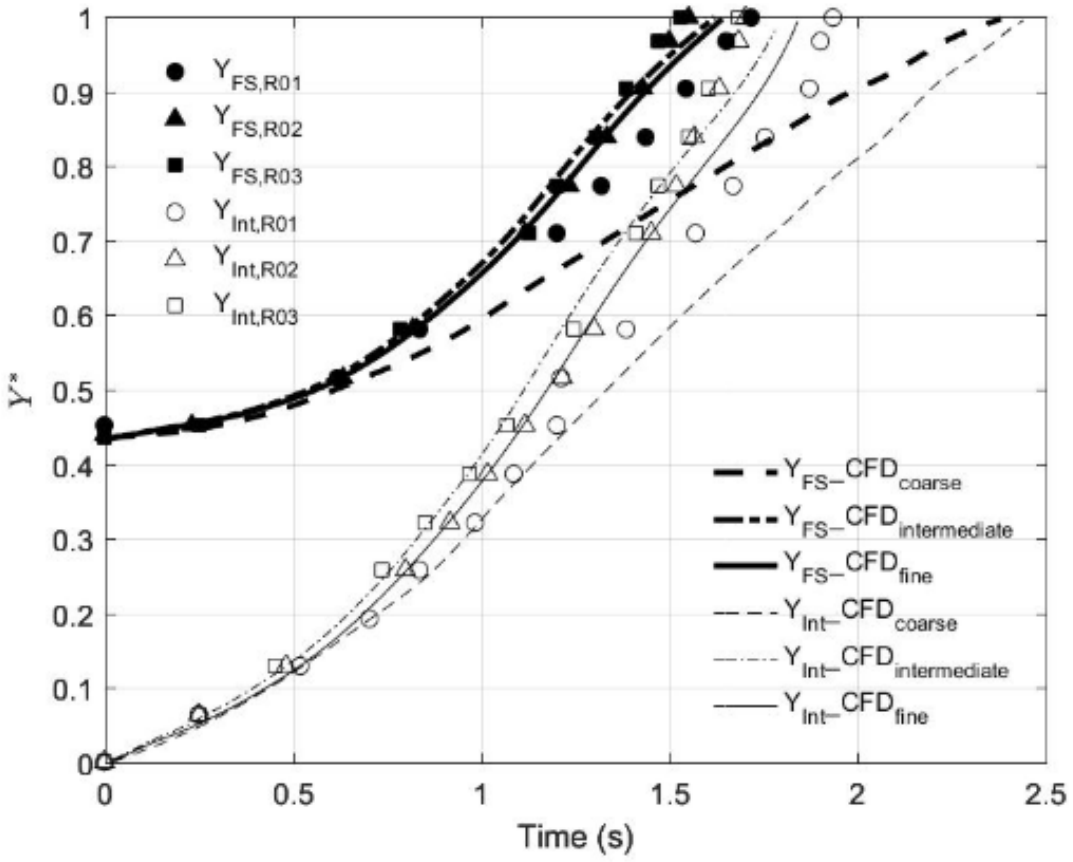

Figure 5.12: Comparison of experimental and CFD model normalized free surface and air-water interface displacement.

Pressure head measured by transducer P3 (normalized by the shaft length L) are compared to CFD predictions at that location in Figure 5.13. In this run, water levels at the shaft were about 1 m above transducer P3 as the air pocket arrived in the shaft. Simulated pressures presented the general trends observed during the experiments. This includes the

sharp pressure drop and rise after the pocket arrival at the shaft and the trend of maximum and minimum pressure head oscillations. Results with the intermediate and fine meshes were similar, and in general yielded a closer match to the events observed in the experiments when compared to the coarse mesh results. Also, CFD-simulated pressure head results never exceeded the shaft rim elevation, even during geysering occurrence. The CFD results were not as accurate as the simulation of the Y_{FS} and Y_{Int}, as there was over-prediction of pressure oscillations magnitude. There was also a time offset between the CFD prediction of the air pocket arrival at transducer P3 and air pocket breakthrough at the shaft rim ranging from 0.1 to 0.2 seconds.

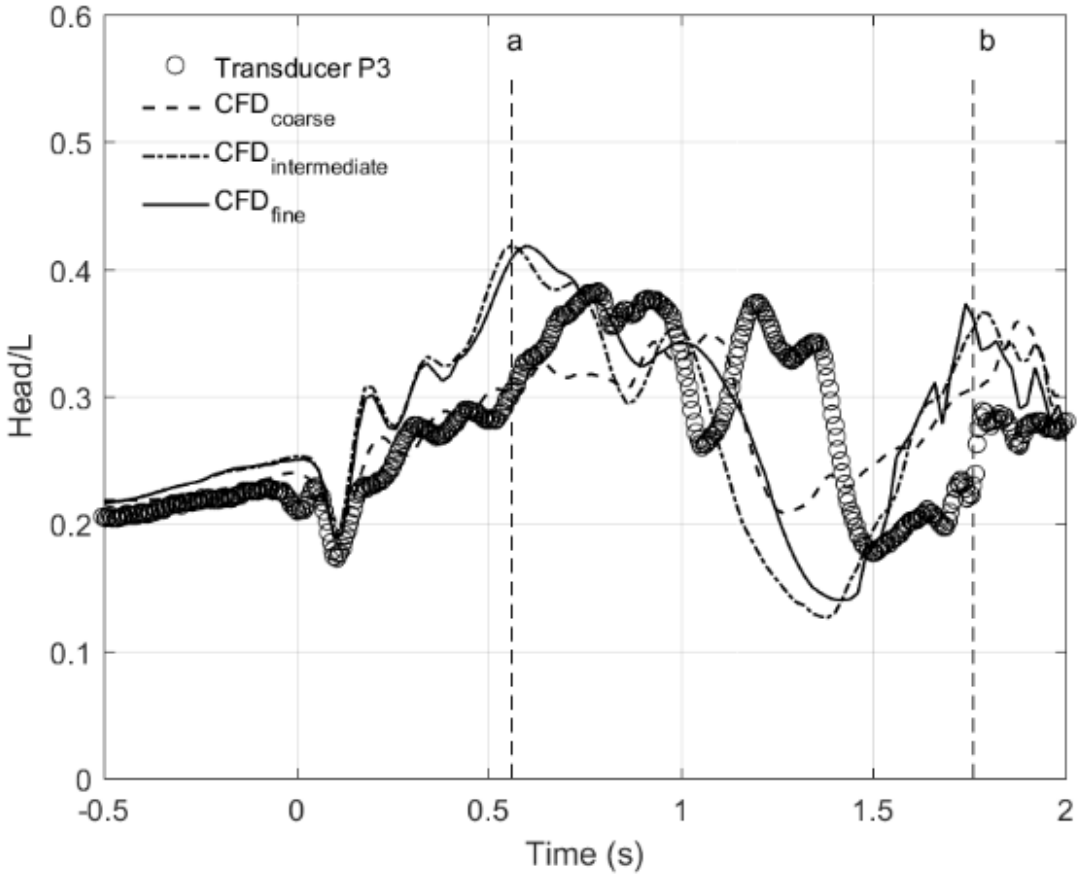

Figure 5.13: Comparison of experimental and CFD model normalized pressure head at transducer P3 on the shaft side. Vertical dashed lines refer to the time in the simulations when a) air pocket leading edge reaches transducer P3 elevation; b) and air pocket breakthrough at shaft rim.

Results from this evaluation were considered positive, particularly with regard to the predictions of the free surface and interface coordinates during air pocket release.

5.5 Extended Shaft

The displacement results from the $V^*_{air} = 3.5$ air pocket in the $D* = 0.67$ shaft, shown in Figure 5.1, were the only cases that did not produce geysers. This led to a proposed solution to mitigate the velocity and magnitude of displacement of both the free surface and the air water interface. Perhaps, by controlling the volume of air that actually entered the tower, geyser occurrence could be reduced.

By extending the base of the $D^* = 0.67$ vertical shaft into the tee joint, presented in Figure 5.14, the amount of air that could enter the vertical shaft was reduced. When a $V^*_{air} = 7.0$ air pocket was released into the system, no geysers occurred, a case that showed geysers in the previous set up. The likely cause of this is the decreased volume of air that was able to enter the pipe.

This decreased the volume of the upward traveling air pocket, which lost momentum before it reached the rim of the vertical shaft, as shown in Figure 5.15. In addition to no geyser occurrence, the velocities also dramatically decreased, displayed in Figure 5.16.

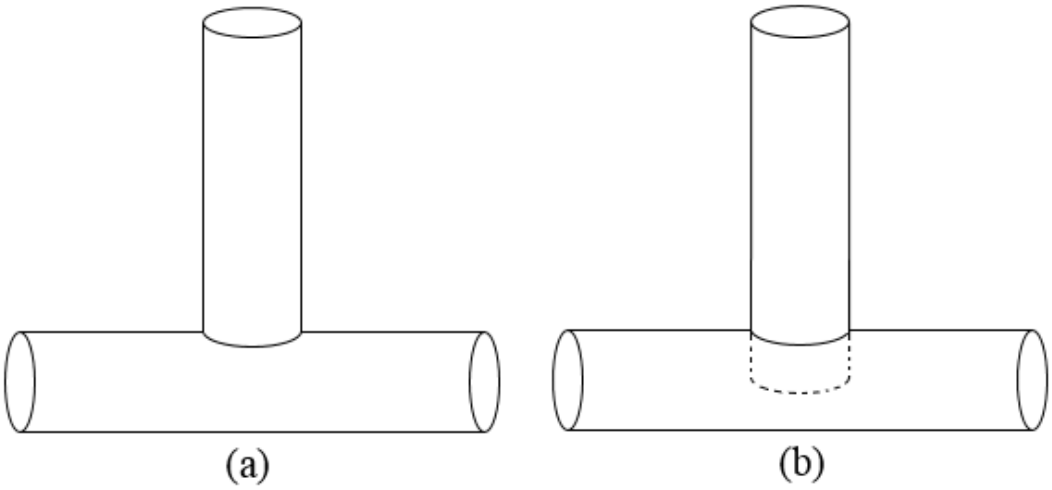

Figure 5.14: (a) The original set up with the shaft meeting at the crown of the pipe. (b) The proposed set up with the shaft extended half way into the cross section of the pipe.

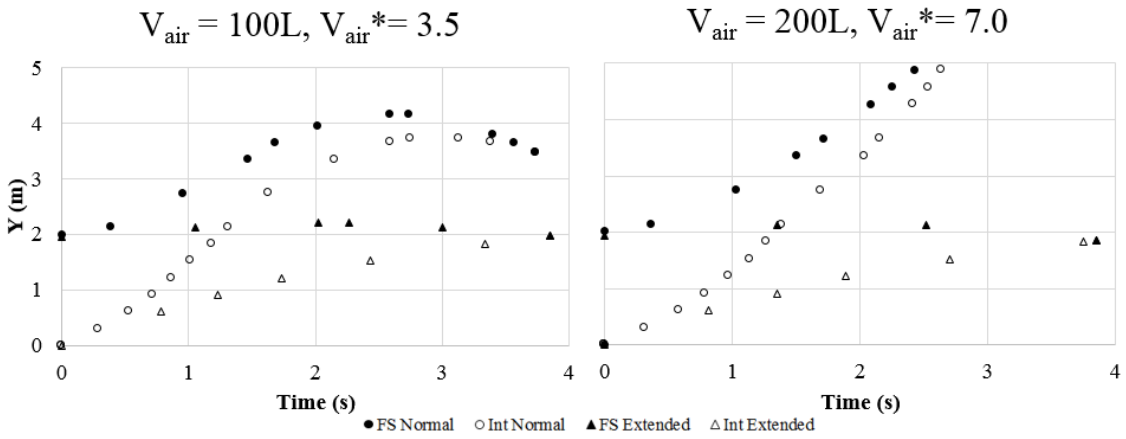

Figure 5.15: Displacement results for shafts extended into the horizontal pipe compared with normal test runs.

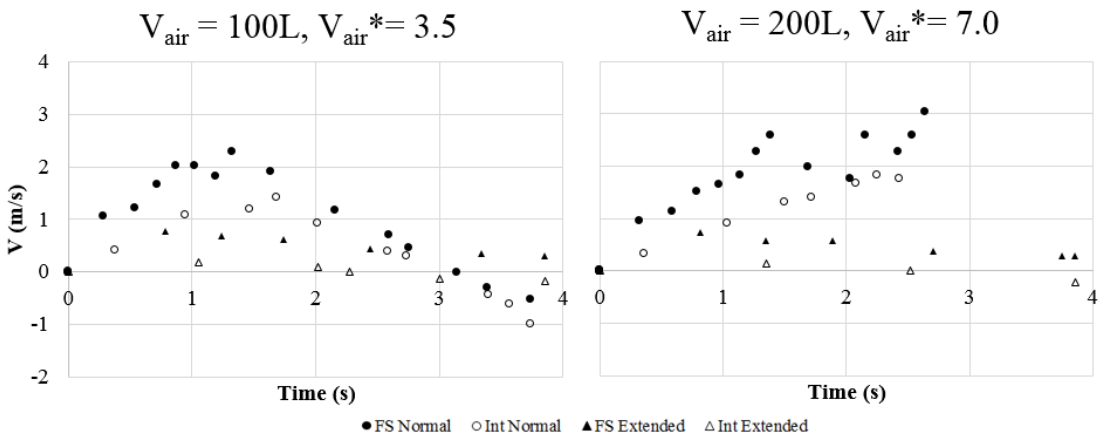

Figure 5.16: Velocity results for shafts extended into the horizontal pipe compared with normal test runs.

5.6 Conclusion

The current work presented results from large-scale experimental tests of the release of large air pocket volumes through water-filled shafts, triggering geysering episodes. While such occurrences are severe and cause serious concern in actual stormwater systems, much is still unknown about geysers and research efforts such as this one are still warranted. Compared to most studies presented to date, the present investigation involved the use of larger diameters for the horizontal and vertical components of the apparatus. The release of air enabled the observation, in some cases, of strong discharges that exceeded several meters in height and had explosive nature. In other cases a mist of very fine water particles was observed when the water slug discharge was complete. These characteristics were not reported in previous studies performed on smaller scales, such as Vasconcelos and Wright [2011].

The understanding of the kinematics of the free surface motion within the shaft and the air-water interface motion is of paramount importance to designers of stormwater systems concerned with the possibility of geysers. The experimental tests have indicated significant displacements of water, even when $D^* = 0.67$, which is consistent with Wright [2013] studies. However, the displacements reported here was larger than the ones measured by Wright [2013], possibly because of the larger initial water level in the vertical shaft. With a better understanding of the displacement of water levels created by varying air pocket sizes and different shaft diameters it will be possible to achieve greater safety in stormwater system designs.

Pressure head measurements during experiments indicate that levels that are within the shaft rim during geyser events, which is consistent with previous investigations. Drops in the pressure measured by transducer P2 at the bottom of the shaft were observed during geyser occurrences. These drops were not as identifiable through the pressure measurements at the lateral of the shaft by transducer P3. This result confirms earlier experimental studies that geysering events can occur when pressure heads are well below grade elevation. Larger swings

of pressure were observed with the two smaller diameters tested, but decreased significantly with the largest D^*. This points to the benefit of having larger diameter shafts in discharging entrapped air pockets in terms of pressure fluctuations after the release.

A CFD model using compressibleInterFOAM solver was created by Jue Wang to represent the same geometry as the experimental conditions from the tests. The tests provided good agreement regarding the kinematic of the water and air-water interface during the air pocket release. The comparison between measured and simulated pressures was not as accurate, however the general trends were well represented.

As it would be anticipated, larger shafts had the ability of capturing larger fractions of air pockets present in horizontal tunnel. CFD results indicated that, for the tested conditions, up to 70% of the entrapped air pocket volume can be admitted in shafts when D^*=1. However, larger shafts presented much smaller vertical displacements of the free surface during air pocket release. Whereas the normalized displacement $\Delta Y_{FS}/Y_{FS,0}$ could be as large as 3 when $D^* \leq 0.5$, this value dropped to a maximum of 1.3 for D^*=1. However, it is important to perform careful CFD simulations of such events, since ΔY_{FS} can be problematic depending on the tunnel geometry. The largest absolute ΔY_{FS} for D^*=1, associated with the largest air pocket volume, reached 26 m. This could pose geyser problems if the tunnel depth is too shallow.

Finally, the velocity of free surface motion increased with air pocket volume and smaller initial water levels in the shaft. These kinematic results of free surface maximum rise and velocity are potentially useful in the context of design of stormwater systems to avoid geysering episodes. For instance, when D^*=0.5 the maximum velocity of the free surface reached 20 m/s during the air release of large pockets through shallow standing water depths in shafts. Such velocities can create problems related to manhole displacements, and further research should investigate this issue with more detail.

There are significant knowledge gaps yet to be addressed in future research. For instance, it would be relevant to measure the pressure within the vertical shaft (i.e. centerline)

during the air release phase, and compare results with CFD results. The use of large scale tests to study the nature of air release in water-filled shafts, both in laboratory and in numerical simulations, should also be considered in future research efforts, along with studies to mitigate geysers in actual stormwater systems

Bibliography

Augustenborg, C.A. and Duke, L.D. (2001). Effectiveness Assessment of NPDES Regulations for Storm Water Discharges. *World Water Congress 2001*, 2001.

Baines, W.F. (1991). Air cavities as gravity currents on slope. *J. Hydr. Eng.*, **117**(12): 1600–1615, 1991.

Batchelor, G. K. (1967). *Introduction to Fluid Dynamics*. Cabridge University Press. Cambridge, U. K.

Baumbach,V. , Hopfinger, E. J. and Cartellier A. (2005). The Transient Behavior of a Large Bubble in a Vertical Tube. *J. Fluid Mech.*, **524**(Vol. A 200): 131–142, 2005.

Benjamin, T.B. (1968). Gravity currents and related phenomena. *J. Fluid Mech.*, 31: 209–248, 1968.

Catano-Lopera, Y., Tokyay, T., Martin, J., Schmidt, A., Lanyon, R., Fitzpatrick, K., Scalise, C., and Garcia, M. (2014) Modeling of a Transient Event in the Tunnel and Reservoir Plan System in Chicago, Illinois. *J. Hydraul. Eng.*, 10.1061/(ASCE)HY.1943-7900.0000888, 05014005.

Chanson, H. (1996). *Air Bubble Entrainment in Free-Surface Turbulent Shear Flows*. Academic Press. London, U. K.

Choi, Y., Leon, A.S., and Apte, S.V. (2014). Three-dimensional numerical modeling of air-water geyser flows. *Proc., 2014 ASCE World EWRI Congress*, 2014.

Chosie, C.D., Hatcher, T.M., and Vasconcelos, J.G. (2014). Experimental and numerical investigation on the motion of discrete air pockets in pressurized water flows. *J. Hydr. Eng.*, 2014.

Cook, M.B., Debell, K.M. (2002). Improving Water Quality in Urban Watersheds. *Linkiign Stormwater BMP Designs and Performance to Receiving Water Impact Mitigation* 24–34, 2002.

Cummings, P.D. and Chanson, H. (1997). Air Entrainment in the Developing Flow Region of Plunging Jets - Part 1: Theoretical Development *J Fluids Eng*, **119**(3): 597–602, 1997.

Davies,R. M. and Taylor,G. I. (1950). The Mechanics of Large Bubbles Rising Through Extended Liquids and Through Liquids in Tubes. *Proc. Royal Soc. London*, **1062**(Vol. A 200): 375–390, 1950.

Goonetilleke, A. Thomas, E., Ginn, S., and Gilbert, D. (2005). Understanding the Role of Land USe in Urban Stormwater Quality Management. *Journal of Environmental Management*, **74**:31-42, 2005.

Guedes de Carvalho, J. R. F., Talaia, M. A. R., Ferreira, M. J. F. (2000) *Flooding instability of high-density gas slugs rising in vertical tubes filled with water. Chem. Engrg. Sci.*, **55**: 3785–3802, 2000.

Guo, Q. and Song, C.S.S. (1991). Dropshaft Hydrodynamics under Transient Conditions. *J. Hydr. Eng.*, **117**(8): 1042–1055, 1991.

Hamam, M.A. and McCorquodale, A. (1982). Transient conditions in the transition from gravity to surcharged sewer flow. *Can. J. Civ. Engrg*, (9): 189–196, 1982.

Lewis, J. W. (2005). *A Physical Investigation of Air/Water Interactions Leading to Geyser Events in Rapid Filling Pipelines*. Ph.D. Thesis. University of Michigan, 2011

Lewis, J.W. and Wright, S.J. (2012). Air-Water Interactions that Generate Large Water Lift through Vertical Shafts in Stormwater Conduits. *J. Water Mngmt. Modeling*, DOI: 10.14796/JWMM.R245-02, 2012.

Li, J. and McCorquodale, A. (1999). Modeling Mixed Flow in Storm Sewers. *J. Hydr. Eng.*, **125**(11): 1170–1180, 1999.

Morgado, A.O., Miranda, J.M., Araujo, J.D.P., Campos, J.B.L.M. (2016). Review on vertical gas-liquid slug flow. *Int. J. Multiph. Flow*, **85**: 348-368, 2016.

McQuillan, K.W. and Whalley, P.B.(1984). Flow patterns in vertical two-phase flow. *Int. J. Multiph. Flow*, **11**(2): 161-178, 1984.

Patrick, A. and Vasconcelos, J. (2015). Air Entrainment Effects on the Pressure Wave Celerities Following Rapid Filling Pipe Flows. *Proc. 2015 ASCE EWRI Congress*, Austin, TX. pp. 1638-1647. DOI: 10.1061/9780784479162.159

Ramezani, L., Karney, B., and Malekpour, A. (2016). Encouraging Effective Air Management in Water Pipelines: A Critical Review. *J. Water Resour. Plann. Manage.*, DOI:10.1061, 2016.

Shaban, H., Tavoularis, S. (2014). Identification of flow regime in vertical upward air-water pipe flow using differential pressure signals and elastic maps. *Int. J. Multiph. Flow*, **61**: 62-72, 2014.

Shammas, N.K., Wang, L.K. (2011) . *Water Supply and Wastewater Removal*. John Wiley & Sons, Inc. Hoboken, NJ.

Shao, Z.S. (2013). *Two-dimensional hydrodynamic modeling of two-phase flow for understanding geyser phenomena in urban stormwater system*. PhD Thesis, University of Kentucky.

Svenungsson, J.(2016). *Solving electric field using Maxwellas equations and compressibleInterFoam solver* Material course at Chalmers University of Technology.

Vasconcelos, J.G. and Wright, S.J. (2006). Mechanisms for air pocket entrapment in stormwater storage tunnels. *Proc., 2006 ASCE EWRI Congress, Omaha, NE*, 2006.

Vasconcelos, J.G. and Wright, S.J. (2008). Rapid flow startup in filled horizontal pipelines. *J. Hydr. Eng.*, **134**(7): 984–992, 2008.

Vasconcelos, J.G. and Wright, S.J. (2009). Rapid filling of poorly ventilated stormwater storage tunnels. *J. Hydr. Res.*, **47**(5): 547–558, 2009.

Vasconcelos, J.G. and Wright, S.J. (2011). Geysering generated by large air pockets released through water-filled ventilation shafts. *J. Hydr. Eng.*, **135**(5): 543–555, 2011.

Wilkinson, D.L. (1982). Motion of air cavities in long horizontal ducts. *J. Fluid Mech.*, 118: 109–122, 1982.

Wright, S.J., Lewis, J.W. and Vasconcelos, J.G. (2011). Geysering in rapidly filling storm-water tunnels. *J. Hydr. Eng.*, **137**(5): 543–555, 2011.

Wright, S.J. (2013). Influence of Air Pocket Volume on Manhole Surge. *J. Water Mngmt. Modeling*, DOI: 10.14796/JWMM.R246-09, 2013.

Hirt, C.W. and Nichols, B.D. (1981). Volume of fluid (VOF) method for the dynamics of free boundaries. *J. Comput. Phys.*, **39**(1): 201–225, 1981.

Weller, H.G., Tabor, G., and Fureby, C. (1998). A tensorial approach to computational continuum mechanics using object-oriented techniques. *Comput. Phys.*, **12**(6): 620–631, 1998.